Article

Performance of a Nanofluid-Cooled Segmented Thermoelectric Generator: Hollow/Filled Leg Structures and Segmentation Effects

Cristian Francisco Ramos-Castañeda [1], Miguel Angel Olivares-Robles [2,*], Ana Elisabeth Olivares-Hernandez [1] and Leobardo Hernandez-Gonzalez [2]

[1] Instituto Politecnico Nacional, Seccion de Estudios de Posgrado e Investigacion, Escuela Nacional de Ciencias Biologicas, Ciudad de Mexico 11340, Mexico; cramosc1201@alumno.ipn.mx (C.F.R.-C.); aolivaresh2100@alumno.ipn.mx (A.E.O.-H.)

[2] Instituto Politecnico Nacional, Seccion de Estudios de Posgrado e Investigacion, Escuela Superior de Ingenieria Mecanica y Electrica Unidad Culhuacan, Coyoacan, Ciudad de Mexico 04430, Mexico; bilbito_98@yahoo.com

* Correspondence: olivares@ipn.mx; Tel.: +52-5554957287

Abstract: A thermoelectric generator (TEG) is studied by considering different leg structures of hollow/filled legs, using new cooling nanofluids, and analyzing the segmentation effect. TEG performance is characterized by power output, conversion efficiency, and exergy efficiency. This study shows the impact of different cooling nanofluids (TiO_2, graphene, and Al_2O_3) on the performance of the thermoelectric generator. Furthermore, in the comparative analysis of nanofluid cooling enhancement for TEG, different hollow/filled thermoelectric legs recently proposed in the literature are considered. Likewise, three segmentation types are used, 2n-2p, 1n-2p, and 2n-1p, thus will be compared with the results of the unsegmented legs. This study calculates the performance of thermoelectric leg structures through a validated numerical simulation on the ANSYS Workbench (modeling, design, and simulation). In addition, the optimal working conditions are evaluated. This study found that quenching of nanofluids can improve TEG performance by up to 17% compared to distilled water. However, the performance improvement of the TEG for each nanofluid is small between them. Furthermore, segmentation of n-type thermocouples improves efficiency and exergy, whereas segmentation of p-type thermocouples improves output power. The segmentation enhances performance by up to twice that of non-segmented leg structures; hollow structures are better performers. In the results, it is reported that the 2n-1p segmentation is the one with the best performance, reaching a maximum energy efficiency of 38%. The triangular leg structure improves performance by up to 75% compared to the rectangular and square leg structures. Likewise, using TiO_2 is the best cooling option with nanofluids since it improves performance by 17% compared to distilled water. Furthermore, the results of cooling nanofluids for TEG performance are useful for the design of thermoelectric leg structures and stimulate further research.

Keywords: exergy; thermoelectric generator (TEG); nanofluids; leg structure variation; numerical simulation; segmentation

1. Introduction

The growing demand for energy and the problems in everyday life caused by the excessive use of traditional energy sources (fossil fuels) have recently caused researchers to look for renewable energy sources and their improvements. This may be achieved by improving the methods of using renewable energy sources and technologies that do not require fossil fuel and by trying to recover some residual energy from thermal processes from industrial plants, cars, and other mobile sources.

When an electric current flows through a thermoelectric generator (TEG), it becomes a heat pump, which transports thermal energy from one side to another: the direction and magnitude of the heat depend on the electric current strength. This phenomenon is known as the Peltier effect [1,2]. The efficiency of a TEG is determined by several factors, including the geometric leg shape of the TEG, the cooling used, and the materials used [3,4].

The leg structure is a critical factor in determining the efficiency of a TEG. Therefore, some research has been conducted on TEGs for leg structure optimization [5–8]. These studies have shown that leg structures of the thermoelectric module significantly influence the device's behavior. Therefore, the leg structure should be designed to maximize the temperature gradient across the TEG. The following summarizes the main results in improving a TEG's efficiency by optimizing the leg structures.

Chen et al. [9] theoretically compared square leg structures with different leg structure dimensions of a solar thermoelectric generator and analyzed the output power and efficiency. The change in the thermal concentration ratio (cross-sectional area divided by substrate area), substrate, and temperature-dependent properties led to an improvement in the performance of the solar thermoelectric generator.

Li et al. [10] investigated a thermoelectric generator's performance, including thermal, mechanical, economic, and exergetic analyses. They examined how hollow cross-sectional leg structures of TEG legs can improve performance and identified the optimal conditions for each case.

Lamba and Kaushik [11] studied a thermoelectric generator (TEG) under the Thompson effect and the leg structure configuration. Using a trapezoidal form, they performed a thermodynamic analysis to evaluate its performance. The conversion energy and exergy efficiency improved by increasing the leg structure parameter but not improving the output power.

Olivares-Robles et al. [12] studied a segmented thermoelectric microgenerator with high-performance nanostructured materials. They considered thermoelements with symmetric and asymmetric leg structures. For a 2p-3n segmented trapezoidal leg structure, it was found that efficiency and output power were improved compared to the conventional rectangular leg structure by 6% and 7%, respectively.

Thimont and LeBlanc [13] found a way to make singular leg structures to optimize thermoelectric device behavior through additive manufacturing in which free-form leg structures are built layer by layer. Their study included the analysis of hollow and prismatic leg structures to find the optimal leg structure design, resulting in higher temperature gradients for hollow and prismatic leg structures, which caused better heat transfer and, therefore, better efficiency.

Zhao et al. [14] performed an energy and exergy analysis on a thermoelectric generator and examined how gas humidification can improve its performance compared to combustion gas generation.

Wiriyasart et al. [15] found that composite fluids enhance the Peltier effect by decreasing the Fourier effect bestowal of the thermoelectric cooler. Therefore, they experimented with a compressed water sink thermoelectric cooling (TEC) module with water, and water solutions of a ferrofluid (Fe_3O_4) and a nanofluid (TiO_2) with concentrations of 0.005% and 0.015%, respectively, to find that Fe_3O_4 had a maximum heat transfer rate of 11.17% and 12.57% compared to TiO_2 and water, respectively.

The cooling method also affects the efficiency of a TEG. The best cooling method removes heat from the TEG as quickly as possible. The use of nanofluids is a promising method for improving the efficiency of TEGs because the nanoparticles in nanofluids increase the thermal conductivity of the base fluid, which can enhance the heat transfer rate in a TEG.

Pfeiffelman et al. [16] studied passive and active cooling and how it affected the performance of a TEG. They concluded that water offers better conditions than air.

Yang et al. [17] studied the different forms of cooling of an annular concentric thermoelectric generator. To improve and analyze the TEG's performance, they used water-cooling,

concurrent air-cooling, countercurrent water-cooling, and countercurrent air-cooling as refrigerants. The maximum net power $P_{net} = 432.42$ W was obtained using countercurrent water-cooling, corresponding to an optimal thermoelectric semiconductor volume of 9.06×10^{-4}.

Olivares-Robles et al. [18] studied the cooling of graphene nanoplatelet aqueous nanofluids (GNAN) in a solar thermoelectric generator, using five different leg structures (three square and two trapezoidal) and several concentrations of the nanofluid to find the optimal leg structure design. They concluded that using GNAN improves up to 15% of the solar thermoelectric generator performance, and efficiency also depends on the leg dimensions.

Abdelkareem et al. [19] sought to take advantage of the residual heat of a TEG; recovering this energy determines the performance of the TEG. Nanofluids were found to significantly improve heat transfer (the Seebeck effect is enhanced by reducing the contribution of the Fourier effect), allowing greater efficiency in their applications.

Ahmed et al. [20] used Al_2O_3 with a weight dispersion of 0.1 and 0.2 vol.% as a coolant on the hot side of a thermoelectric cooler (TEC), showing a 40% improvement in the coefficient of performance TEC for concentrations of 0.2 vol.%.

He Ruan et al. [21] performed an analysis and performance comparison between a TEG and a TEC using graphene, Al_2O_3, and CuO nanofluids. They concluded that using nanofluids improves the TEC's performance coefficient more than the efficiency of the TEG.

Xing et al. [22] showed that graphene nanoplatelets could reduce nanofluid deposition and standardization. The simulation used thermoelectric and liquid modules in an Ansys Workbench environment. GNAN was used as a coolant on the TEG's cold side to achieve a better heat transfer. The results showed that the heat, efficiency, output power, and voltage of the hot surfaces of the TEG system were increased by the liquid nano coolant.

Chen et al. [23] studied and compared the differences between microfluid, multi-fluid, and nanofluid and the applications that can be given to each; finding the different applications each can have and how they improve the performance or manufacturing of devices.

Sundar et al. [24] studied the effective thermal conductivity and viscosity of the magnetized nanofluid Fe_3O_4/water. The thermal conductivity and viscosity of the nanofluid increased with a rise in particle concentration. However, the viscosity improvement was more significant than the improvement in thermal conductivity at the same volume concentration and temperature.

Kaushik and Manikandan [25] investigated the exo-reversible thermodynamic model of an annular thermoelectric generator (ATEG) and considered the Thompson, Peltier, Fourier, and Joule effects using an exergy analysis. They concluded that an ATEG has a lower efficiency to that of a TEG.

Tian et al. [26] proposed the segmented annular thermoelectric generator as an efficient structure. Although it has not been commercialized yet, they concluded that the segmented model is better than a conventional one regarding efficiency and power output.

Kedher et al. [27] studied the combined effects of using a rotating cylinder and a shear-thinning nanofluid to improve the performance of a cabinet installed with a TEG with multiple ventilation ports. They used two nanofluids, which they called NF1 and NF2. They found that using NF1 improved behavior by up to 49%, and when using NF2, it improved by up to 61%.

Various studies on TEGs are focused on applications such as automotive, aerospace, industrial, and everyday life [28–30].

Other studies [31–36] seek to improve the performance of a thermoelectric generator from different approaches, such as mechanical stress analysis, hybridization of the system, and the use of phase change materials (PCM).

The optimization of the leg structure, the use of nanofluids, and the materials used are all promising methods for improving the efficiency of TEGs. The optimization of these

factors can lead to significant improvements in the efficiency of TEGs, which can make them a more viable option for renewable energy generation.

The novelty of this work lies in the comprehensive performance analysis of a TEG using ANSYS simulation. This study considers the leg structure configuration and the impact of nanofluids on the TEG to obtain the optimal leg structure. The output power, efficiency, and exergy efficiency results are presented as a function of heat flux and area ratio for water and various nanofluids. Additionally, this study compares the results with different segmentation methods. Overall, this work provides insights into the design optimization of TEGs for enhanced performance and efficiency.

In this work, in Section 2, performance analysis of a TEG is conducted via ANSYS simulation, where the leg structures, material parameters of cooling liquids, and governing equations are the input quantities. The results for the output power, efficiency, and exergy efficiency as a function of the heat flux and area ratio for water and various nanofluids are presented in Section 3, and the results are compared with different segmentations. Our results are obtained by considering the leg structure configuration and the influence of nanofluids on the TEG to obtain the optimal leg structure. Finally, in Section 4, the conclusions are presented.

2. Methods and Materials

2.1. Physical Model and Assumptions

The results of our study are compared with previous results by employing computational analysis.

Parameters such as the coordinate system, material properties, and input parameters are set to compare the established leg structures and analyze their effect on TEG performance.

This study investigates the effect of various cooling nanofluids on the thermal performance of a TEG with triangular hollow/filled leg structures. The nanofluid coolants considered for improving TEG efficiency are distilled water, graphene, Al_2O_3, TiO_2, and Fe_3O_4 at a weight concentration of 0.1%-wt.

The model of a TEG is composed of two semiconductor legs (p-type and n-type) connected with copper and two layers of ceramic insulation that are bonded to the hot and cold sides of the thermoelectric generator. The scheme of the thermoelectric generator and the leg structures considered in this work are shown in Figure 1. In addition, the dimensions of the study by Min Li et al. [10] are considered in our study.

The model includes thin solder layers between the legs, and the thermal analysis considers the copper interconnections.

Figure 1b shows the five different hollow leg structures considered, namely, square, rectangular, octagonal, circular, and triangular, with their corresponding sizes.

A part of the cross-sectional area is removed from the semiconductors' inside, forming ring-shaped legs. The leg structure cross-sectional area base (A_0) is between 1 and 2 mm^2.

The ratio of the interior hole area to the total area ($R_A = A_i/A_0$) for all leg structure configurations is 0.5 (unless otherwise stated). Therefore, the height of all the legs used is 1.5 mm. Bi_2Te_3 is selected as the material for the n-type and p-type semiconductors. A detailed scheme of thermoelectric legs in a ring-shaped structure is shown in Figure 1b [10]. In addition, temperature-dependent properties of Bi_2Te_3 were considered to increase the accuracy of the simulations. The analysis included the elastoplastic behavior of the carrier layers and copper interconnections because it has a relaxing effect leading to reduced thermal stress on the thermoelectric legs. In addition, the analysis considers the Thompson effect, but the temperature dependence of electrical and thermal resistance is constant.

The best materials for TEGs are those with a high Seebeck coefficient and a low thermal conductivity. The most common materials used in TEGs are bismuth telluride, lead telluride, and silicon germanium. We use $PbTe$ and Bi_2Te_3 as semiconductor materials, p-type, and n-type. Figure 2 shows the properties of the materials dependent on temperature (Thermal

conductivity, Figure 2a; Seebeck coefficient, Figure 2b; Electrical resistivity, Figure 2c; and Merit figure, Figure 2d).
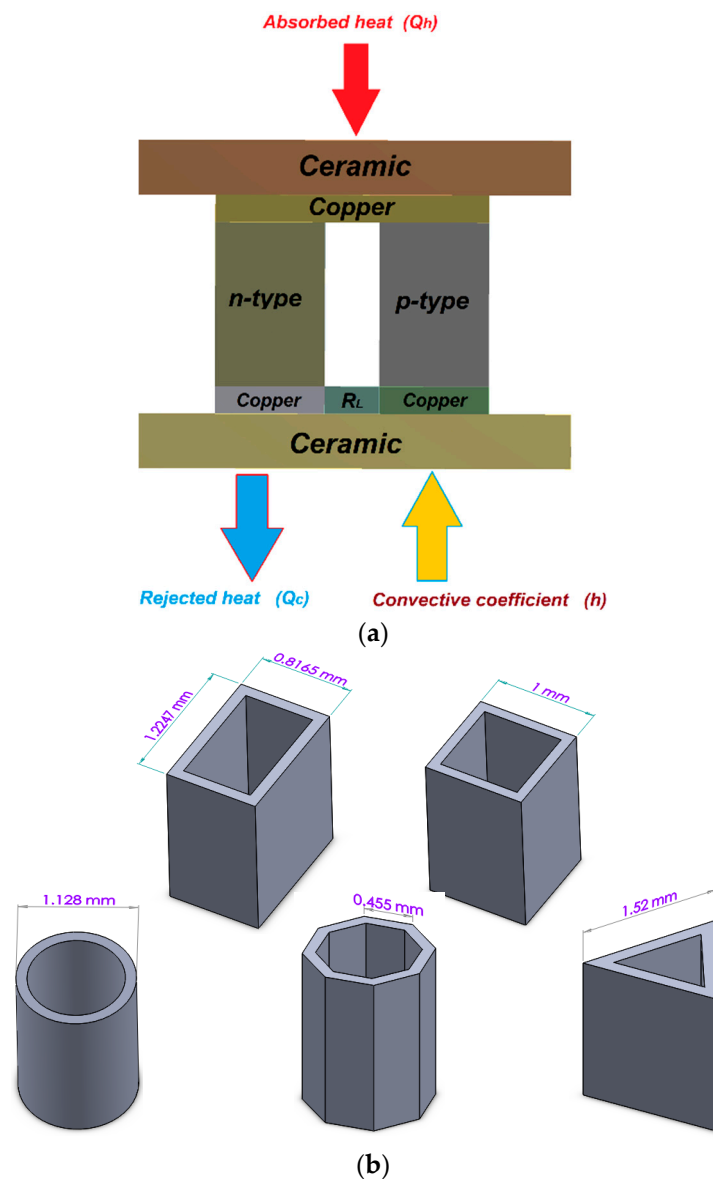

(a)

(b)

Figure 1. (**a**) Scheme of the thermoelectric generator with the load resistance R_L. (**b**) General view of the mesh with Dimensions of the leg structures.

PbTe and Bi_2Te_3 are two common materials used in the construction of segmented thermoelectric generators. The behavior of these materials in different temperature ranges is critical to their efficiency and performance.

PbTe is a narrow-bandgap semiconductor material with a high thermoelectric figure of merit (Image), in the mid-temperature range between 600 and 800 K. PbTe has a relatively high melting point and is chemically stable, making it an excellent choice for high-temperature applications. However, *PbTe* has low *ZT* values at low temperatures, and its performance decreases at temperatures above 900 K due to the formation of undesirable secondary phases. Therefore, PbTe is typically used in segmented structures, where the temperature range can be optimized to take advantage of its high *ZT* values.

On the other hand, Bi_2Te_3 is a wide-bandgap semiconductor material with a high *ZT* value in the low-temperature range between 300 and 400 K. Bi_2Te_3 is less chemically stable than PbTe, but its performance remains relatively constant over a wide temperature

range. However, Bi_2Te_3 has a low melting point, which limits its use in high-temperature applications.

Simple hollow and layered leg geometries can result in larger temperature gradients and higher output power than the traditional cuboid structure. This dependence on thermal resistance and power output on leg geometry offers a compelling rationale for investigating additive manufacturing techniques for thermoelectric devices.
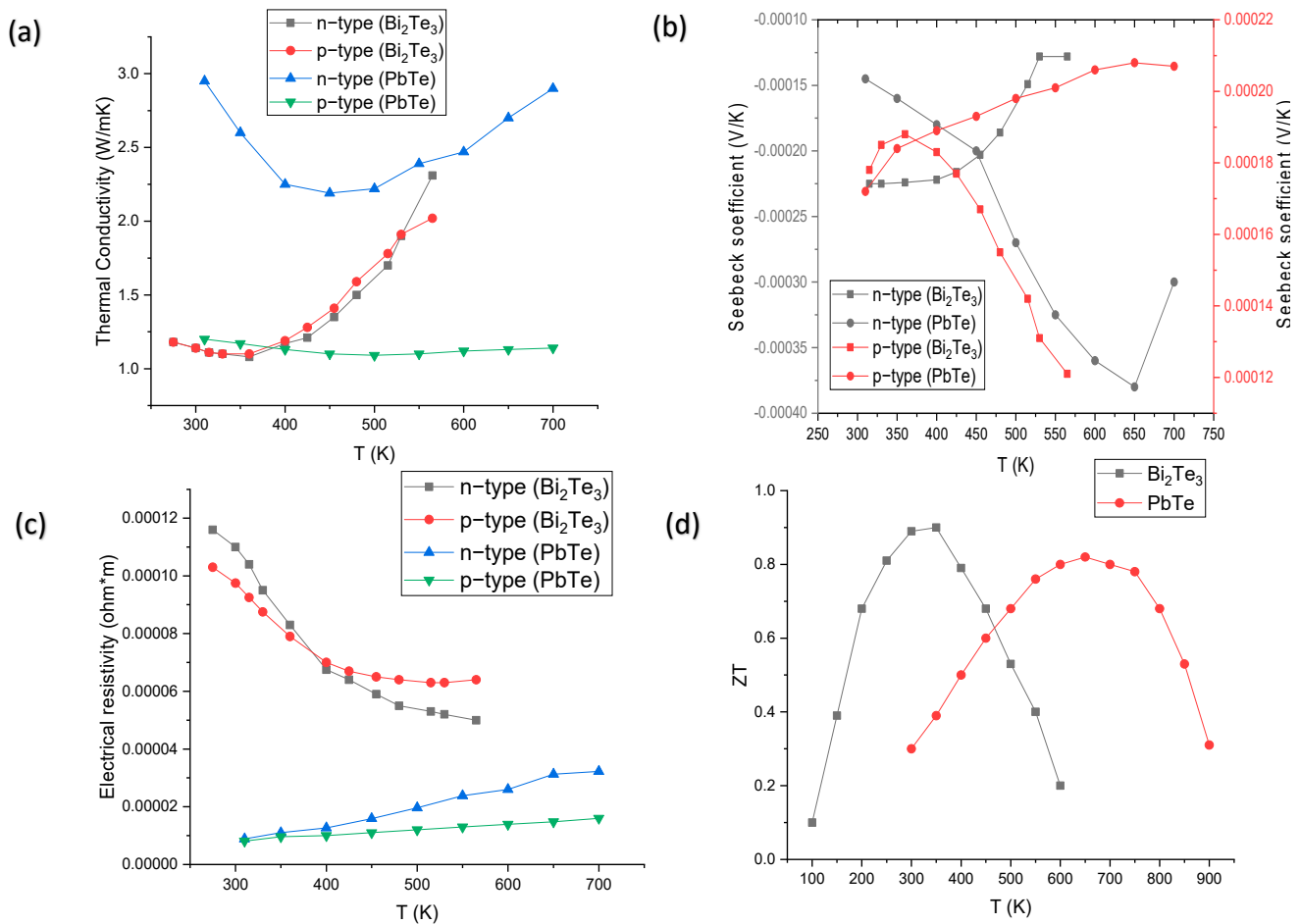

Figure 2. Properties of material dependent on temperature. (**a**) thermal conductivity, (**b**) Seebeck coefficient, (**c**) electrical resistivity, and (**d**) merit figure.

The leg structure significantly affects the temperature difference and electrical potential across the leg. Compared to their filled counterparts, the heat transfer rate is reduced in the hollow and layered geometries, resulting in higher effective thermal resistance. The increase in thermal resistance for the hollow structure is primarily due to the impact of the leg geometry on the thermal resistance. These thermal trends also extend to the open circuit voltage developed across each leg geometry, as the electrical potential is directly related to the temperature gradient.

Therefore, segmented structures made from both materials can be designed to take advantage of their specific temperature ranges, resulting in a higher overall efficiency for the thermoelectric generator.

2.2. Numerical Method and System Performance

Figure 3 shows the mesh distribution that was made for the TEG.
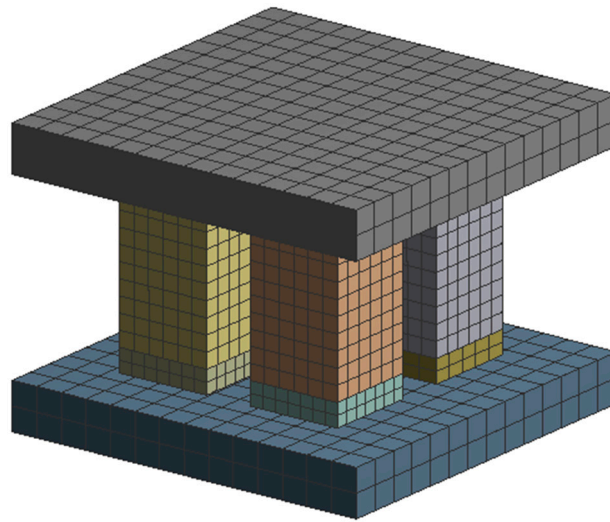
Figure 3. General view of the mesh.

The performance analysis of a TEG in the stationary state is carried out with the thermoelectric module of the ANSYS Workbench. In addition, a network independence test is carried out to minimize the uncertainty of the simulations. Voltage values for various total elements tested are shown in Table 1.

Table 1. Mesh independence results in various elements.

Number of Nodes	Voltage (V)
22,940	0.25569
45,880	0.25569
68,820	0.25569
91,760	0.25568
114,700	0.25567

Semiconductors, interconnections, insulators, and grip layer properties are listed in Tables 2 and 3. K, α, R, and β are the thermal conductivity, Seebeck coefficient, electrical resistance, and coefficient of thermal expansion, respectively.

Table 2. Properties of Bi_2Te_3 elements [10].

Properties	n-Type	p-Type
k (Wm^{-2}K^{-1})	$2.24 \times 10^{-8}(T-T_0)^3 + 7.09 \times 10^{-6}(T-T_0)^2 - 1.26 \times 10^{-2}(T-T_0) + 4.09$	$-3.31 \times 10^{-8}(T-T_0)^3 + 7.29 \times 10^{-5}(T-T_0)^2 - 3.79 \times 10^{-2}(T-T_0) + 7.12$
α (VK^{-1})	$1.46 \times 10^{-11}(T-T_0)^3 - 1.50 \times 10^{-8}(T-T_0)^2 + 5.14 \times 10^{-6}(T-T_0) - 8.12 \times 10^{-4}$	$-2.96 \times 10^{-11}(T-T_0)^3 + 3.11 \times 10^{-8}(T-T_0)^2 - 1.08 \times 10^{-5}(T-T_0) + 1.48 \times 10^{-3}$
R (Ωm)	$-2.13 \times 10^{-13}(T-T_0)^3 + 1.42 \times 10^{-10}(T-T_0)^2 + 1.09 \times 10^{-8}(T-T_0) - 2.1 \times 10^{-6}$	$-7.60 \times 10^{-13}(T-T_0)^3 + 7.78 \times 10^{-10}(T-T_0)^2 - 1.93 \times 10^{-7}(T-T_0) - 1.8 \times 10^{-5}$
$\beta\left(K^{-1}\right)$	$-3.408 \times 10^{-16}(T-T_0)^4 + 9.317 \times 10^{-13}(T-T_0)^3 - 9.246 \times 10^{-10}(T-T_0)^2 + 3.96 \times 10^{-7}(T-T_0) - 4.894 \times 10^{-5}$	$-3.408 \times 10^{-16}(T-T_0)^4 + 9.317 \times 10^{-13}(T-T_0)^3 - 9.246 \times 10^{-10}(T-T_0)^2 + 3.96 \times 10^{-7}(T-T_0) - 4.894 \times 10^{-5}$

Table 3. Properties of copper interconnectors, wielding, and ceramic layers [13].

Properties	Copper	Ceramic Layers	Wielding Layers
k $(\mathrm{Wm}^{-2}\mathrm{K}^{-1})$	385	25	55
R $(\Omega\mathrm{m})$	1.69×10^{-7}	1×10^{-12}	5×10^{-8}
$\beta\left(\mathrm{K}^{-1}\right)$	1.7×10^{-5}	0.68×10^{-5}	2.7×10^{-5}

2.3. Governing Equations

The governing equations are solved by Galerikin's finite element method, which is a numerical approximation method [37].

The following equations governing the system and relating the thermal and electric fields define the thermoelectric material's behavior.

$$\nabla\cdot\left(\alpha T \vec{J}\right) - \nabla\cdot(k\nabla\mathrm{T}) = \vec{J} \tag{1}$$

$$\nabla\cdot\left(\frac{1}{\rho_e}\vec{E}\right) - \nabla\cdot\left(\frac{\alpha}{\rho_e}\nabla T\right) = 0 \tag{2}$$

where α is the Seebeck coefficient, T is the temperature, $\vec{E}$ is the electric field, $\vec{J}$ is the vector current density, and P_e and k are the thermoelement's resistivity and thermal conductivity [18].

The physical scales of temperature, T, and electric scalar potential, ϕ, over a computational element are approximated by:

$$T = [N]\{T_e\} \tag{3}$$

$$\phi = [N]\{\varphi_e\} \tag{4}$$

where N, T_e, and φ_e are the element shape function, the nodal temperature vector, and the nodal electrical potentials vector, respectively.

Integrating Equations (1) and (2), the differential equations can be written algebraically:

$$\begin{bmatrix} K^{TT} & 0 \\ K^{\varphi T} & K^{\varphi\varphi} \end{bmatrix} \begin{Bmatrix} T_e \\ \varphi_e \end{Bmatrix} = \begin{Bmatrix} Q^L \\ I^L \end{Bmatrix} \tag{5}$$

Where Q^L and I^L are the thermal load vector and the electric current load vector, respectively. K^{TT}, $K^{\varphi T}$, and $K^{\varphi\varphi}$ are the thermal stiffness matrix, the Seebeck stiffness matrix, and the electric stiffness matrix, respectively, and can be defined as:

$$K^{TT} = \int_v \nabla N\cdot[k]\cdot\nabla N dV \tag{6}$$

$$K^{\varphi T} = \int_u \nabla N\cdot\left[\frac{1}{\rho_e}\right]\cdot[\alpha]\cdot\nabla N dV \tag{7}$$

$$K^{\varphi\varphi} = \int_u \nabla N\cdot\left[\frac{1}{\rho_e}\right]\cdot\nabla N dV \tag{8}$$

The equations are solved using the commercial software ANSYS. Then, the calculations are repeated until the convergence criteria are satisfied. Convergence is defined when the relative temperature and electric potential differences between two iterations are less than 10^{-6}; this minimal difference is enough to ensure a stable simulation according to some numerical reference.

The heat flow equation for thermoelements is as follows:

$$q = \kappa \nabla T + \alpha J T \tag{9}$$

$$I = \frac{\alpha \Delta T}{R_L + R} \tag{10}$$

$$P_{out} = I^2 \cdot R_L = Q_h - Q_c \tag{11}$$

where V_{OC} is the open-circuit voltage, α is the Seebeck coefficient, ΔT is the temperature difference between the cold side and the hot side, R_L is the load resistance, and P_{out} is the output power.

The equations used to calculate the efficiency and exergy are the following [10]:

$$\eta = \frac{P_{out}}{Q_h} \tag{12}$$

$$Ex_{in} = Q_h \left(1 - \frac{T_0}{T_h} \right) \tag{13}$$

$$\zeta = \frac{P_{out}}{Ex_{in}} \tag{14}$$

where η is the energy efficiency, T_0 is the room temperature, T_h is the temperature of the hot side, Q_h is the absorbed heat from the hot side, Ex_{in} is the exergy used to generate the power [14], and ζ is the exergy efficiency.

2.4. Boundary Conditions

The boundary conditions established for the analysis of these models are the temperature of the cold side, which is set at 298.15 K, and the temperature of the hot side, which varies from 325.15 K to 548.15 K, having a $\Delta T_{MAX} = 250$ K. Voltages of 0 V and 0.08 V are established on the n-type and p-type semiconductor copper electrodes, respectively.

Equations (1) and (2) can be solved simultaneously using the three-dimensional space finite element method. With Equations (1), (2), and (9) we can find the equations for heat transfer from the hot side (Q_h) and the cold side (Q_c).

$$Q_h = \alpha_h I T_h - \frac{I^2 R}{2} + K(T_h - T_c) \tag{15}$$

$$Q_c = \alpha_h I T_c - \frac{I^2 R}{2} + K(T_h - T_c) \tag{16}$$

where K is the thermal conductance, R is the electrical resistance, I is the electrical current, T_h is the temperature of the hot side, and T_c is the temperature of the cold side.

The Fourier heat, Peltier heat, and contact Joule heat are described in Equations (15) and (16). According to basic thermoelectric theories:

$$V_{OC} = \alpha \Delta T \tag{17}$$

The cold side is at the bottom of the TEG (25 °C) for the cooling process, while the heat is transferred from the hot side. Therefore, the ambient temperature (T_0) was 20 °C.

2.5. TEG and Nanofluid System

This study analyzes the improvement of thermal cooling on the cold side of thermoelectric cooling for a segmented TEG. Water, TiO_2 nanofluid, graphene, Al_2O_3, and Fe_3O_4 ferrofluid with 0.1% concentration were selected because they are the refrigerants already studied in previous literature [15,18–20]. The properties of nanofluids (Table 4) signifi-

cantly influence the improvement of heat transfer. Viscosity is one of the most important properties to maintain optimal performance of the TEG because if the concentration of nanoparticles in the nanofluid is increased, it would be more viscous and would impair heat transfer since the refrigerant would not flow properly and would overheat.

Table 4. Properties of nanofluids [18–20,24], thermal conductivity (κ), kinematic viscosity (ν), density (ρ), and specific heat (C_p).

	κ/W·m^{-1}·K^{-1}	ν/10^{-7}m^2·s^{-1}	ρ/kg·m^{-3}	Cp/J·kg^{-1}·K^{-1}
Distilled water	0.6	7.47797	997	4181.7
TiO$_2$	0.607	9.2143	1048	3502
Fe$_3$O$_4$	0.6274	8.174939	1003.06	4178.485
Al$_2$O$_3$	0.661	10.07544	1007.4	4154.7
Graphene	0.752	9.97062	1123.3	3343.188

For simulation purposes, a convective boundary condition based on the thermophysical properties of the nanofluid is established on the cold side of the TEG, as shown in Figure 1a.

The nanofluid passes through the bottom of the cold side of the TEG. Therefore, the area where nanofluid passes is assumed to be equal to the substrate area of the TEG.

Suppose the refrigerant is detected in the laminar flow development stages, and the influence of different physical properties is negligible. In this case, the Zader–Tate equation can describe the Nusselt number with a distance of 0.052 m [18].

$$Nu = 1.86\left(\frac{RePr}{l/de}\right)^{1/3} \tag{18}$$

where $Pr = \rho\nu Cp/\kappa$ is the Prandtl number, $Re = ude/\nu$ is the Reynolds number, and $de = 4A_f/B$ is the equivalent diameter. In those equations, ν is the kinematic viscosity, u is the flow, A_f is the viscosity, κ is the thermal conductivity, B is the wet perimeter, and $h_L = \kappa Nu/l$ is the heat transfer coefficient.

Heat loss from semiconductors and thermal resistances in the cooling tube and ceramic plates are ignored. The convective values are added to the input parameters for simulation purposes, and a convective boundary condition is established based on the nanofluid's thermophysical properties. We will use graphene, Al_2O_3, TiO_2, and Fe_3O_4 dispersed in a fluid. In particular, the hollow triangular leg structure was also cooled with nanofluids' weight dispersion of 0.1%-wt. Table 4 shows the properties of the nanofluids used. The weight concentration in nanofluids is 0.1%. The dispersion stability of nanofluids is not considered in the numerical analysis.

Nanoparticles such as TiO_2, graphene, and alumina are commonly used as coolants in thermoelectric generators because they have high thermal conductivity and can enhance the heat transfer performance of the cooling fluid. In addition, these nanoparticles have unique properties that can improve the performance of the thermoelectric generator.

For example, TiO_2 has a high thermal conductivity and is chemically stable, making it an excellent choice for improving the heat transfer performance of the coolant. Graphene has high electrical conductivity, high mechanical strength, and a large surface area, which can enhance the material's thermoelectric properties. Alumina has a high thermal conductivity and is also chemically stable, making it suitable for use as a coolant in harsh environments.

Overall, the choice of nanoparticle coolant depends on various factors, including the specific application, the thermoelectric materials used, and the desired performance of the thermoelectric generator.

2.6. Validation Method: Performance of TEG with Distilled Water Cooling

Using output parameters that the ANSYS Workbench gives as a result of the simulations and Equations (11) and (12), the output power and conversion efficiency are calculated as a function of the heat flow in the TEG. Figure 4a shows the previously published results by the Min Li methodology [10] for method validation. Figure 4b shows the thermodynamic performance of the TEG with filled leg structures. The numerical simulation shows that hollow forms offer better performance than filled ones under the following conditions: cold side temperature is fixed at 25 °C, load resistance of 0.0212 Ω, and it is stationary for the simulation. In addition, the triangular leg structure has higher power output and energy conversion for all heat flows. Therefore, the triangle leg structure is the best choice under the given conditions.
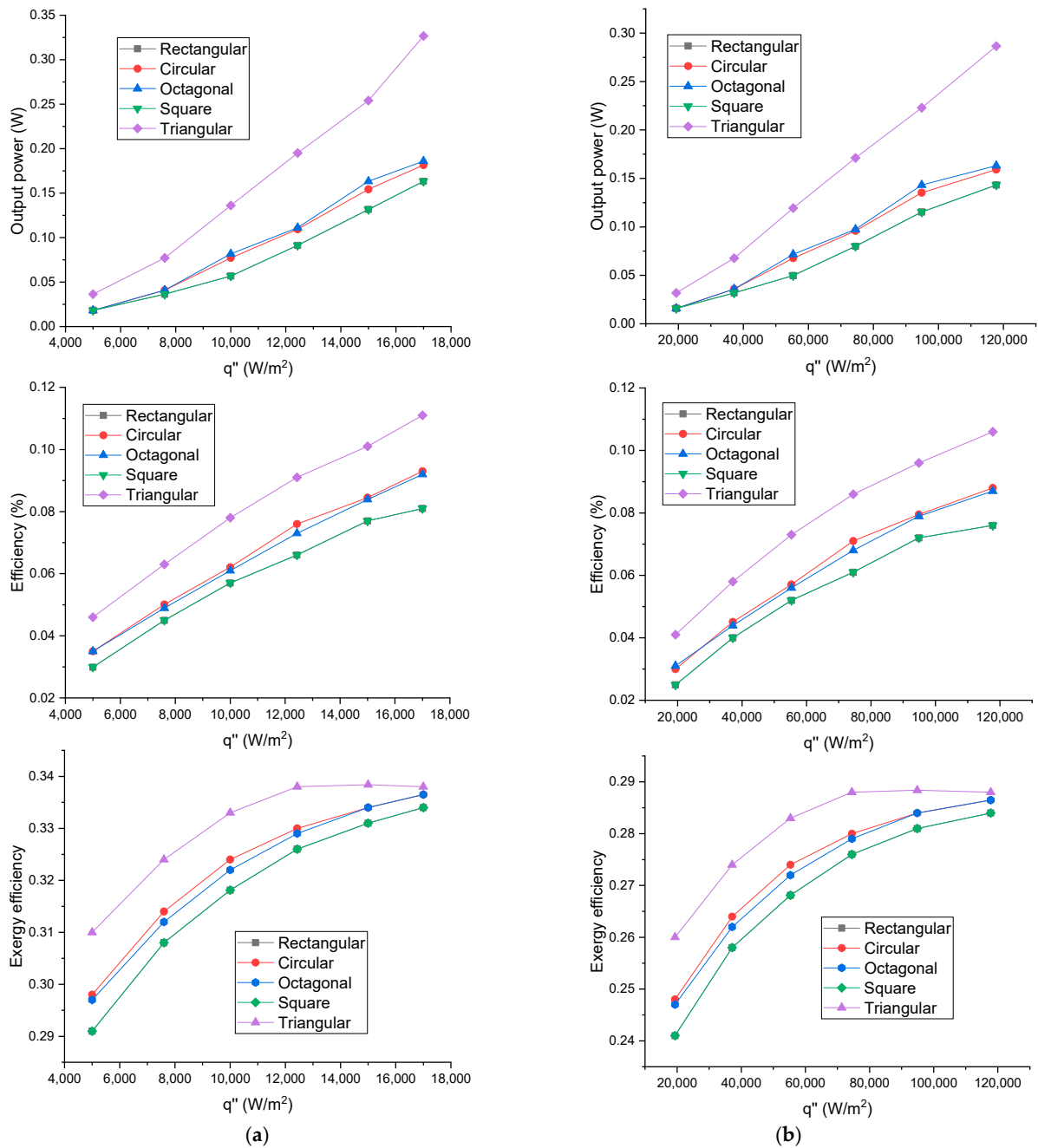
Figure 4. Output power, energy efficiency, and exergy efficiency as a function of heat flux for (**a**) hollow [10] and (**b**) solid legs (validation).

The best leg structure is the triangular one, and the hollow leg structures present greater power output than filled leg structures.

Table 5 shows all hollow and filled leg structures' output power, efficiency, and maximum exergy efficiency values.

Table 5. Performance for hollow and filled leg structures with a heat flux of 17 kW/m^2 and 120 kW/m^2, respectively.

Structure	Output Power (W)		Efficiency		Exergy Efficiency	
	Hollow	Filled	Hollow	Filled	Hollow	Filled
Triangular	0.28656	0.072	0.111	0.106	0.338	0.288
Square	0.14328	0.036	0.081	0.076	0.334	0.284
Octagonal	0.16318	0.041	0.093	0.088	0.3365	0.2864
Circular	0.1592	0.04	0.092	0.087	0.3364	0.2864
Rectangular	0.14328	0.036	0.081	0.076	0.334	0.284

In particular, the exergy efficiency of a TEG is a function of the output power and Q_h, as defined by Equations (11) and (12).

The triangular leg structure also provides a higher exergy efficiency in function of the heat flux. However, when the cold side temperature rises, all the leg structures (except the square one) give approximately the same exergy efficiency values.

All curves show a monotonic value increase except for the triangular leg, which presents a maximum of 12 kW/m^2 and 74.5 kW/m^2 for hollow and filled legs. This maximum value may be significant for TEG design. Remarkably, the increment rate of output power (due to the increment of heat flux) in the triangular leg structure is sharper compared to the other leg structures, which shows the suitability of the triangular leg structure for higher-range heat fluxes.

Exergy efficiency converges for high values of heat flux, which is important for design criteria and limits the operation of thermoelements in the TEG.

Regarding the improved performance of hollow leg structures over filled ones, there are several reasons:

- Reduced thermal conductivity: Hollow leg structures have lower thermal conductivity compared to filled leg structures. This lower thermal conductivity reduces heat transfer through the legs, allowing for better temperature gradients and improved energy conversion.

- Minimized parasitic heat losses: Hollow leg structures provide a barrier between the hot and cold sides of the thermoelectric generator, reducing parasitic heat losses. By minimizing heat transfer to the surroundings, more heat can be utilized for power generation, resulting in improved performance.

- Increased surface area: The presence of the hollow cavity in the leg structure increases the effective surface area available for heat exchange. This larger surface area facilitates better heat dissipation and more efficient heat transfer, contributing to improved overall performance.

Overall, the triangular leg structure offers advantages such as enhanced heat transfer, reduced thermal resistance, improved electrical potential, while the hollow leg structures provide benefits such as reduced thermal conductivity and minimized parasitic heat losses. These factors collectively contribute to the superior power output, energy conversion, and exergy efficiency observed in the triangular leg structure and the hollow leg structures, respectively.

3. Results

For this study, what is of interest are the steady-state results, so a transient-state analysis or study was not considered.

In this section, we begin showing our results for the best hollow leg structure of the thermoelectric legs proposed by Min Li [10] but cooled with different nanofluids. Figure 5 shows the temperature distribution for the triangular leg structure with 16 thermoelements. Similar behavior is obtained for the other leg structures. The ambient temperature is the cold side temperature (298 K) up to 540 K for the hot side.
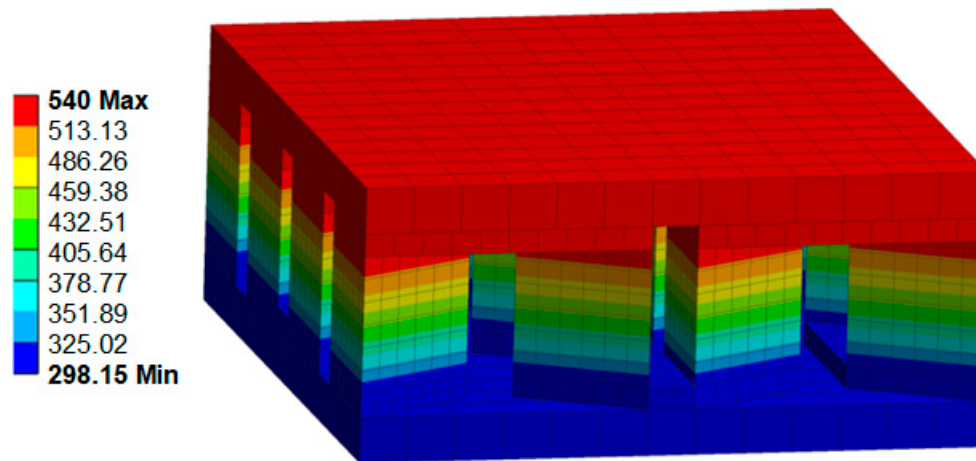

Figure 5. Temperature distribution of triangular leg structure with 16 thermoelements.

3.1. Performance of the Thermoelectric Generator with Hollow Triangular Legs with Different Cooling Nanofluids

The triangular shape is often used in thermoelectric generators because it allows for efficient heat transfer and reduces thermal resistance, improving performance compared to other geometries.

In a thermoelectric generator, electricity is produced by exploiting the temperature difference between the hot and cold sides of the device. The efficiency of this process depends on how effectively heat can be transferred from the hot side to the cold side.

In a triangular shape, the triangle's base serves as the hot side, while the two sloping sides form the cold side. This design allows for a larger surface area on the cold side, increasing the heat transfer rate and reducing thermal resistance. In addition, the sloping sides of the triangle allow for more uniform temperature distribution, further improving performance.

The triangular leg structure in a thermoelectric generator has been found to achieve better power output, energy conversion, and exergy efficiency compared to other leg structures for several reasons [10,13,14]:

- Enhanced heat transfer: The triangular leg structure provides increased surface area for heat transfer compared to other geometries such as square, circular, octagonal, or rectangular. This larger surface area facilitates better heat dissipation, resulting in improved thermal performance and higher power output.
- Reduced thermal resistance: The triangular leg structure has a lower thermal resistance compared to other leg structures. This reduced resistance allows for more efficient heat flow through the legs, minimizing heat losses and maximizing energy conversion.
- Improved electrical potential: The triangular leg structure promotes a larger temperature gradient across the legs, which directly relates to the electrical potential difference. This enhanced temperature gradient leads to higher voltage generation, contributing to better power output and energy conversion.

Other geometries, such as rectangular or cylindrical shapes, may not have as large a surface area on the cold side, leading to higher thermal resistance and reduced efficiency. However, it is worth noting that the optimal geometry for a thermoelectric generator will depend on the specific application and operating conditions.

Figure 6 shows the output power as a function of heat flux. Notice that TiO_2 was the nanofluid that presented the best results, although not by a relevant difference compared to Al_2O_3. The maximum power output of the TEG using Al_2O_3 is 0.407 W, while TiO_2 is 0.41 W, and Fe_3O_4 is 0.393 W at 17 kW/m^2. The output power increase using nanofluids compared to water is 15%, 16.53%, 17.32%, and 12.57% using graphene, Al_2O_3, TiO_2, and Fe_3O_4, respectively.
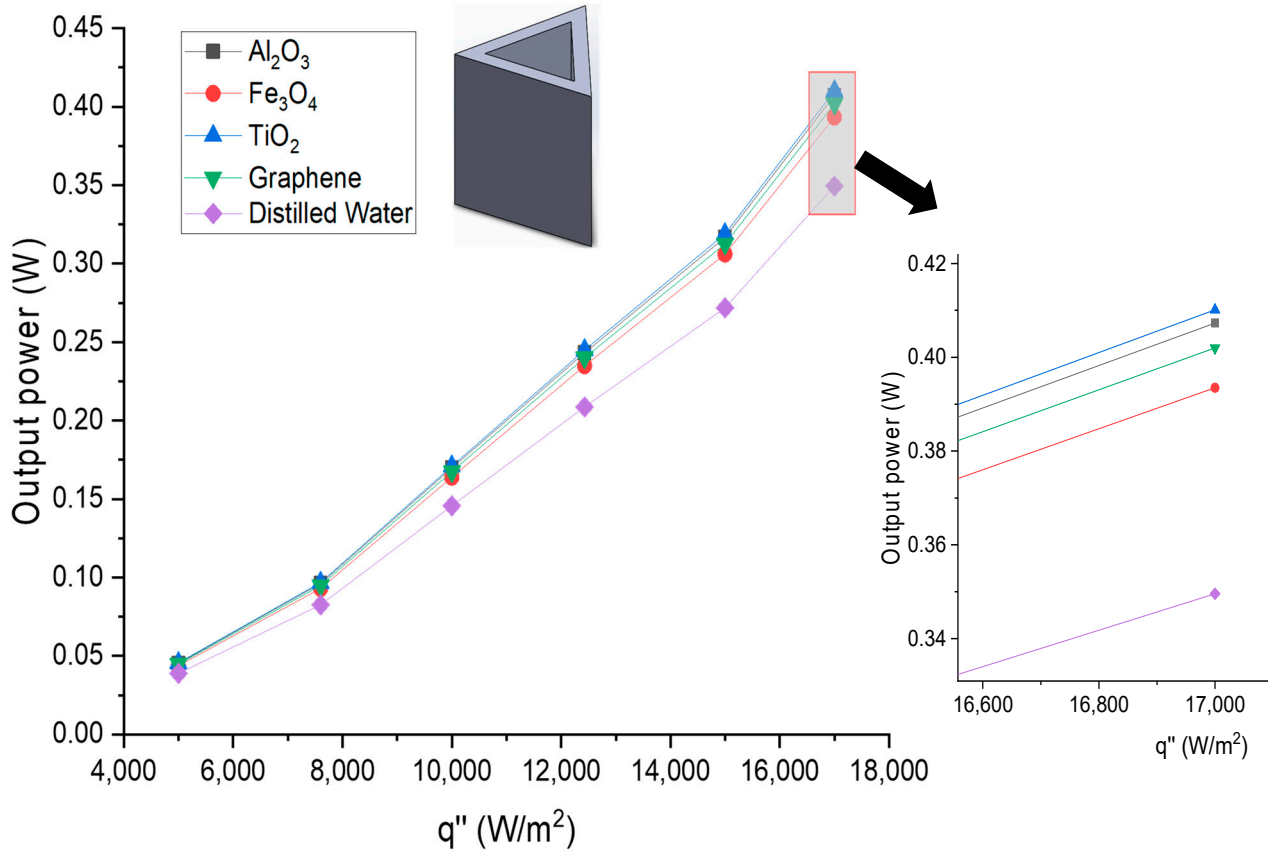

Figure 6. Output power as a function of heat flux for the hollow triangular leg structure with different nanofluids.

Figure 7 shows the efficiency versus heat flow using different nanofluids. The efficiency at 17 kW/m^2 for Al_2O_3, TiO_2, Fe_3O_4, and graphene is 0.123, 0.124, 0.119, and 0.121, respectively. The nanofluid that offers the best efficiency is TiO_2, and compared to Fe_3O_4, which is less efficient, results in a difference of 5.04×10^{-4}.

Increasing the temperature of the cold side increases the input exergy, but the output power decreases (Equation (11)). Due to this, the exergy efficiency is expected to decrease. Therefore, the cold side temperature increases, and the exergy efficiency of the TEG of circular and triangular leg structures is reduced by up to 27%.

Figure 8 shows the exergy efficiency of the TEG for several nanofluids with hollow triangular leg structures.
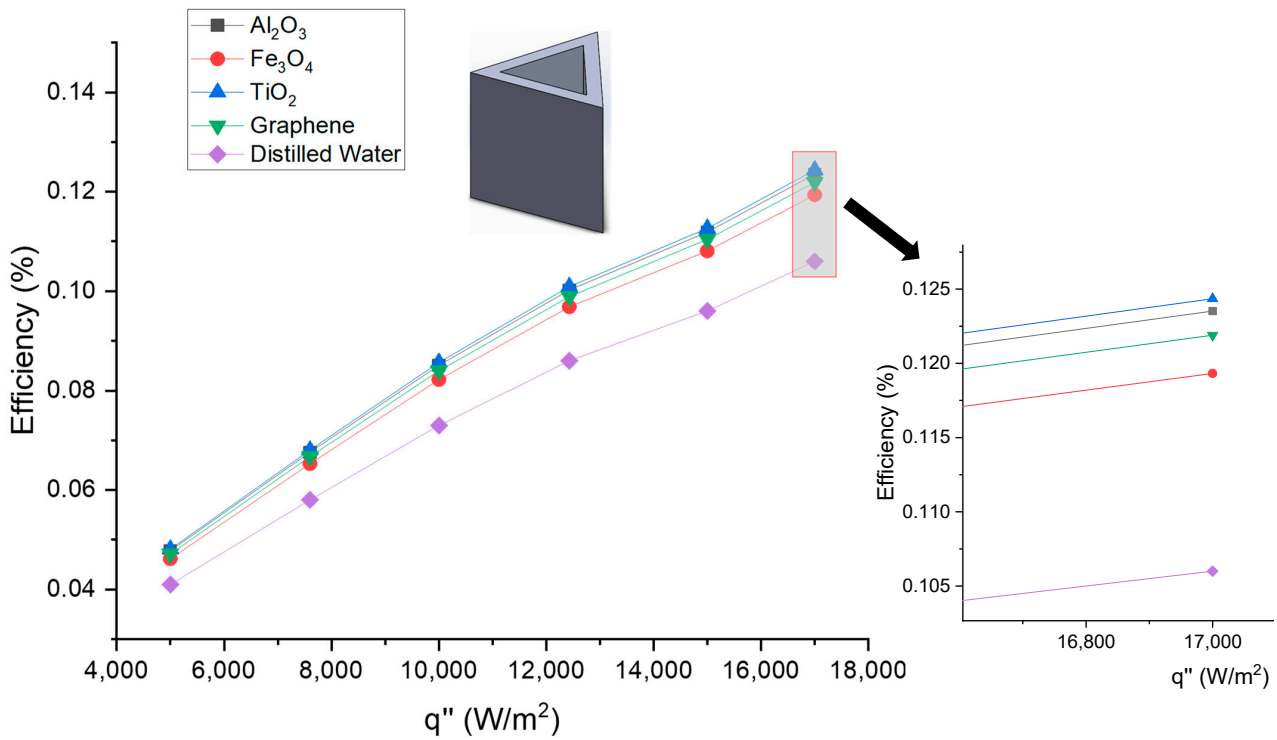
Figure 7. Energy efficiency for hollow triangular leg structure with different nanofluids as a function of heat flux.
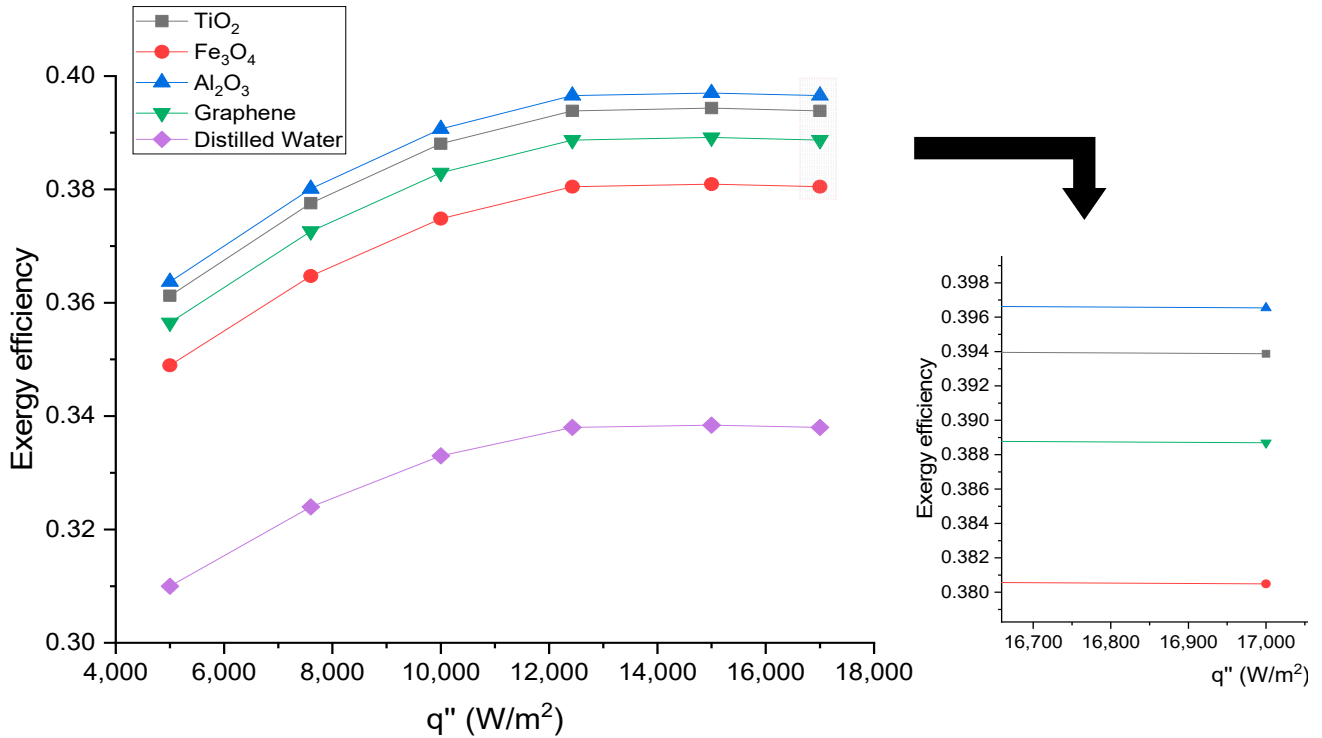

Figure 8. Exergy efficiency for the hollow triangular leg structure with different nanofluids as a function of heat flux.

The change in efficiency using different cooling nanofluids is noticeable. The increase in efficiency is 0.013 between TiO_2 and Fe_3O_4, and between TiO_2 and distilled water, there is an efficiency difference of 0.05. The exergy efficiency of TiO_2 is 0.396 at 17 kW/m^2. Remember that exergy is the most valuable work obtained from a given transfer of energy. Therefore, the difference in exergy efficiency between nanofluids is significant. Using nanofluids in a TEG can improve performance by up to 20%. Table 6 shows the maximum output power, efficiency, and exergy values for distilled water and the nanofluids used for the triangular leg structure. Compared with the work of He Ruan [21], who used TiO_2 at 0.1%-wt and reached a maximum TEG efficiency of 6.5%, ours reaches up to 12% TEG efficiency, using a 0.1% TiO_2-wt.

Table 6. Output power, efficiency, and exergy for the distilled water and nanofluids used for triangular leg structure.

	Output Power (W)	**Efficiency**	**Exergy**
Distilled water	0.34956	0.106	0.338
Graphene	0.40198	0.1219	0.3887
Al$_2$O$_3$	0.40731	0.12352	0.39387
Fe$_3$O$_4$	0.3935	0.11932	0.38049
TiO$_2$	0.4101	0.12436	0.39654

The Carnot factor and the conversion efficiency are affected by the temperature of the heat source and sink as well as the height ratio (Section 2.2). Increasing the heat source temperature T_h enhances the conversion efficiency, as mentioned, but the Carnot factor grows as well. Taking this into account, between these two conflicting factors, the outcome is determined by the dominant factor. For a specific range of height ratios with the increase of source temperature, the increase of the Carnot factor is more than the enhancement of conversion.

The difference between distilled water and nanofluids is significant since performance can be improved by up to 20%, but the difference in nanofluids is practically negligible.

Notice that the TEG performance with Al_2O_3 nanofluid as coolant outperforms the TEG performance using the other four nanofluids. Table 6 shows the numeric values for the hollow triangular leg structure with different cooling nanofluids.

Figure 9 shows the output power and energy efficiency as a function of the area ratio. The higher the area ratio, the higher the power output and efficiency, meaning the more gap, the better performance the TEG will have. Again, TiO_2 is higher compared to the other nanofluids.

3.2. TEG: Segmentation Effect

This section studies the effect of the segmented hollow/filled leg structures on the performance of the thermoelectric generator using cooling nanofluid. The segmentation materials in each leg are Bi_2Te_3 and $PbTe$. Each segment has a height of 0.75 mm, and the measurements are the same as those observed in Figure 4. As in the previous sections, we consider hollow leg structures now segmented. Figure 10 is the meshed schematic diagram for segmented leg structures. Figure 10c shows the measurements of the segmented models. When 2n-1p segmentation is used, the n-type semiconductor is segmented in half with a length of 0.75 mm each, while the p-type semiconductor has a length of 1.5 mm.
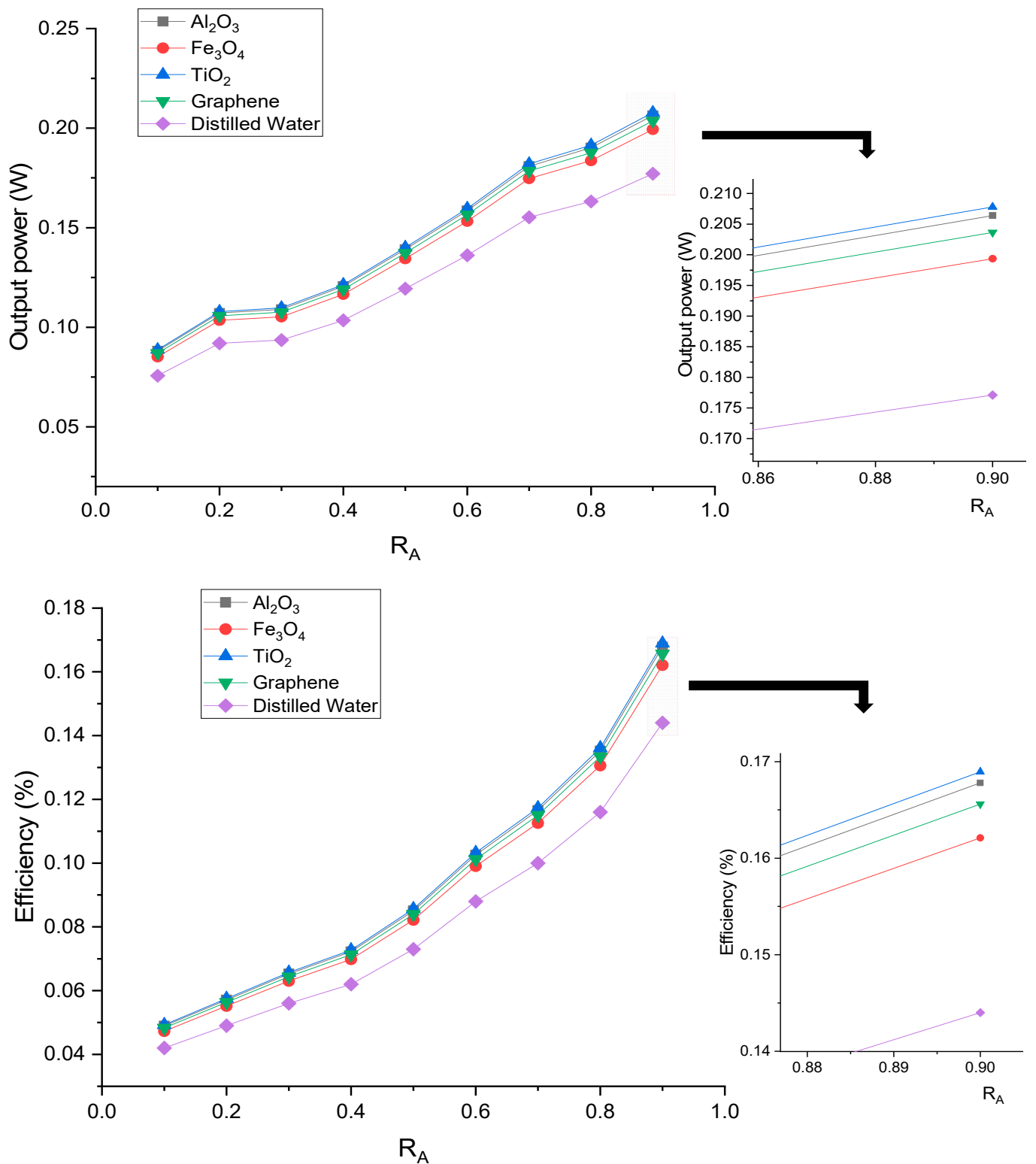
Figure 9. Output power and efficiency as a function of area ratio for hollow triangular leg structure with different nanofluids. The effect of the ratio of hollow inner area to total area (R_A) on power generation (heat flux = 17 kW/m^2).
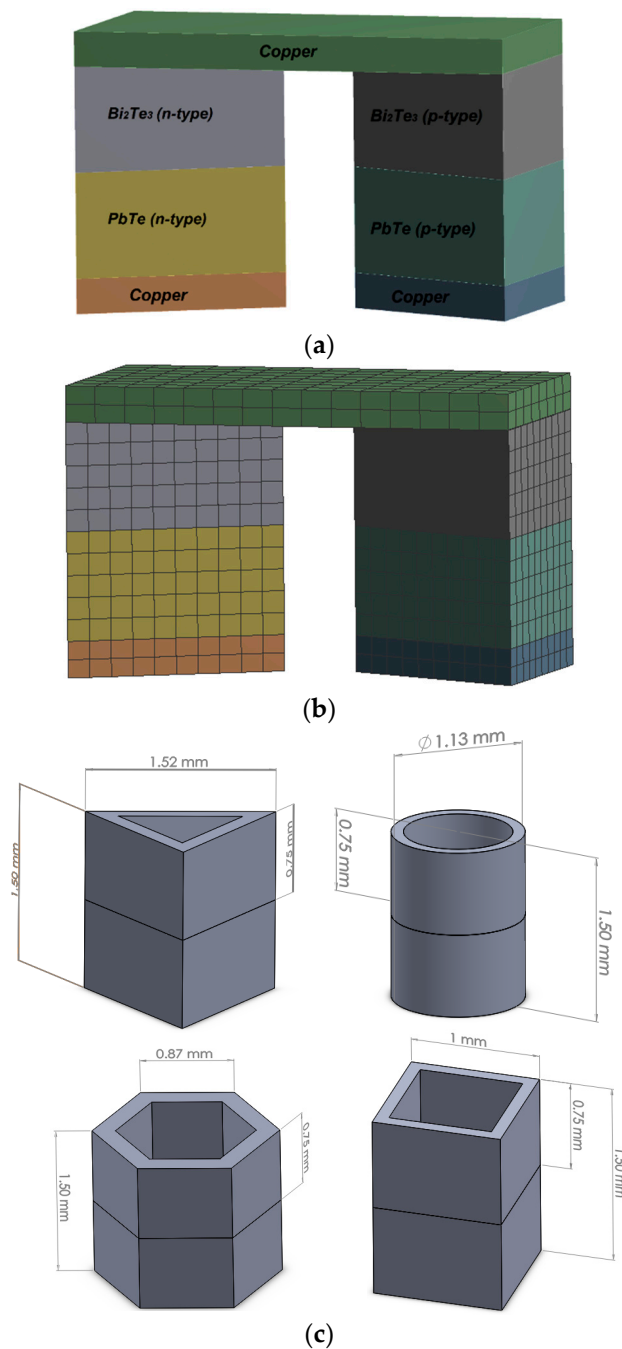
Figure 10. (**a**) Schematic diagram of segmented triangular leg structures, (**b**) view of the adaptive meshing, and (**c**) dimensions of the geometries used for segmentation analysis.

The segmentation is 0.75 mm for all leg structures. The external area is one mm^2, and the total height is 1.5 mm. The models were in the SOLIDWORKS software and were later imported to ANSYS Workbench to carry out the pertinent analyses.

Each segment typically consists of two materials with different thermoelectric properties in a segmented thermoelectric module. When a temperature gradient is applied across the module, an electrical current is generated due to the difference in the Seebeck coefficient between the two materials.

The temperature gradient is a measure of the change in temperature over distance, and its magnitude and direction can affect the performance of the thermoelectric generator. For example, if the temperature gradient is too high, it can cause thermal stresses that can

damage the material. On the other hand, if the temperature gradient is too low, it may not be sufficient to generate enough electrical power.

To optimize the performance of a segmented thermoelectric module, it is important to carefully design the module's geometry, as well as the materials used and their doping levels, to achieve the desired temperature gradients and maximize the system's efficiency.

The ΔT_{max} of Bi_2Te_3 is 250 K, while that of $PbTe$ is 400 K. The simulations must consider this since the material can be overheated and not have optimal performance results.

Four different analyses are carried out for the case of segmented thermoelements. The first is to analyze it without segmentation. The second is to segment both thermocouples in half. The third is to segment the n-type thermocouple in half and leave the p-type normal. Finally, the fourth is to segment the p-type thermocouple in half and leave the n-type normal.

The output power, energy efficiency, and exergy efficiency are calculated for these cases regarding the heat flow.

3.2.1. Segmentation Effect with Distilled Water

Figure 11 shows differences in the segmented leg structures. The power output of the segmented square leg structure is below the non-segmented triangular leg structure, which reinforces the relevance of leg structure for TEG analysis.
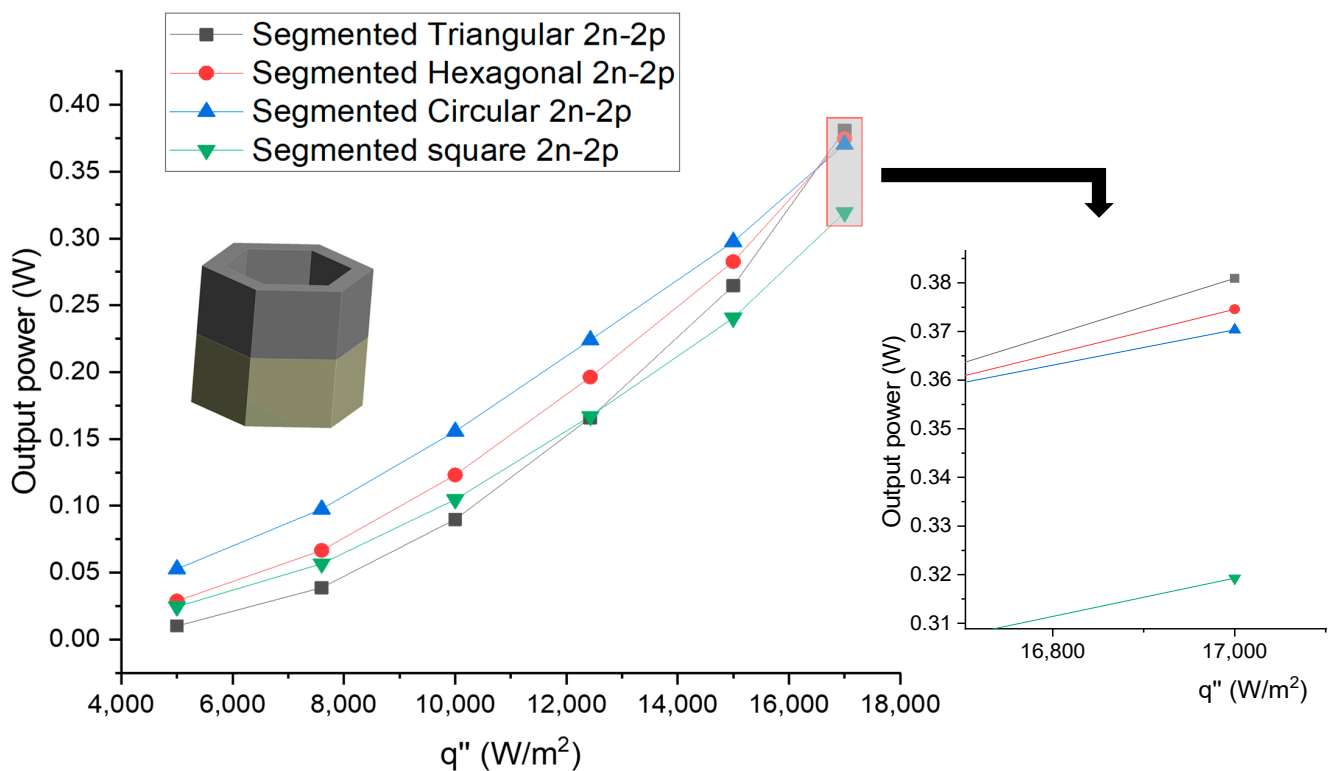

Figure 11. Output power as a function of heat flow for hollow segmented leg structures with distilled water.

For the hollow leg structures, the best structures are the segmented circular and square, with a maximum efficiency of 13.222 and 13.18%, respectively, and the maximum efficiency of the segmented triangular leg structure is 13.159%. This is due to the geometry of the segmented leg structures and the materials used in the semiconductor elements. Figure 12 shows that the segmented circular leg structure now has the highest maximum efficiency (13.125%) for solid leg structures, while the triangular structure is 13.104%.
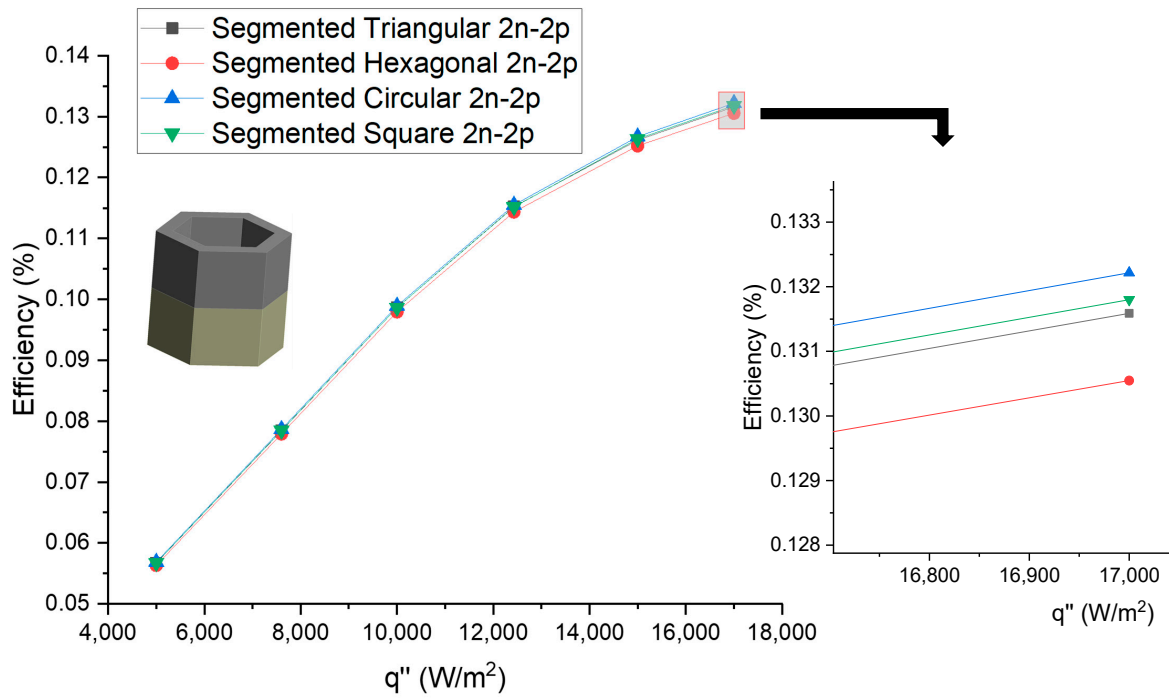
Figure 12. Energy efficiency as a function of heat flow for hollow segmented leg structures with distilled water.

The exergy efficiency of segmented leg structures is lower than the structures that are not segmented; additionally, the circular leg structure is the best in segmented leg structures with a maximum exergy efficiency of 0.300. Figure 13 shows the exergy efficiency for the segmented leg structures.
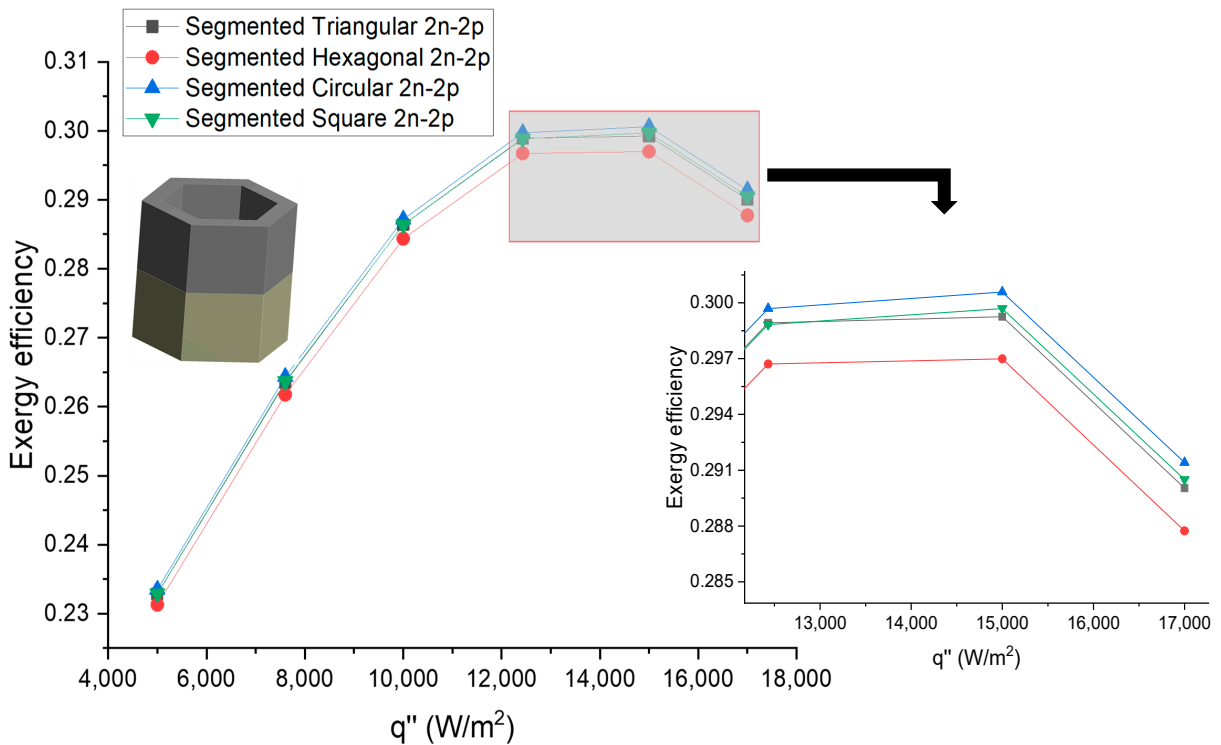

Figure 13. Exergy efficiency as a function of heat flow for hollow segmented leg structures with distilled water.

In Appendix A, the analysis for the four different segmentations is studied, and it is shown that the 2n-1p segmentation is the optimal segmentation for the performance of the TEG. It is also shown that the circular and triangular leg structures have the best performance, so they are compared with each other using TiO_2 as a refrigerant. This agrees with the conclusion of Ref. [12].

3.2.2. Segmentation Effect with Cooling Nanofluid

In this case, since in the previous results of this study TiO_2 turned out to be the optimal nanofluid for TEG's performance compared with distilled water, the output power, energy efficiency, and exergy are analyzed for hollow leg structures.

The exergy improves with nanofluids, which allows us to choose the appropriate nanofluid depending on the application.

Figure 14a shows that segmenting leg structures improves power output compared to that obtained by Min Li [10]. Notice that the circular structure with segmentation 2n-1p has the best output power for heat flux values less than 12 kW/m^2. While after 12 kW/m^2, the triangular leg structure with 2n-1p segmentation has better power output.
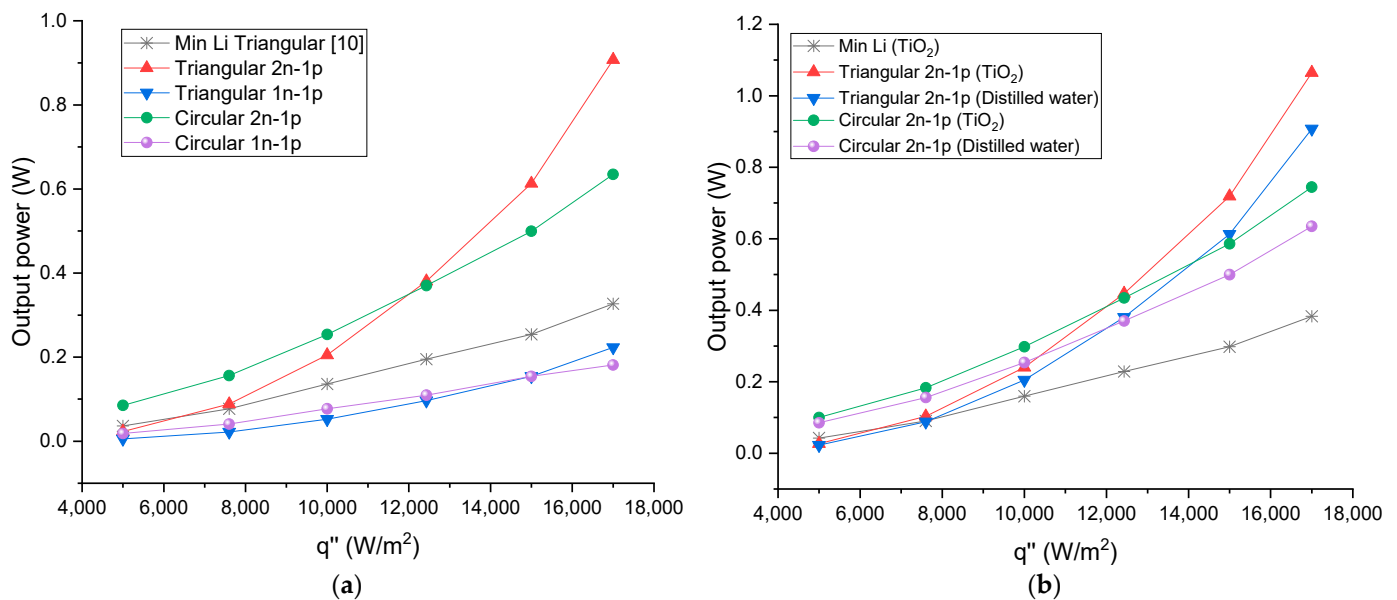

Figure 14. Output power for circular and triangular leg structures with two different segmentations compared with Min Li results; (**a**) distilled water as coolant and (**b**) TiO_2 as coolant.

Compared with Min Li's study with a maximum output power of 0.326 W, the output power is two times better for circular 2n-1p segmentation and three times better for triangular 2n-1p segmentation for a heat flow of 17 kW/m^2 with 0.634 W and 0.907 W, respectively, as shown in Table 7.

Figure 14b shows the output power improvement using TiO_2 nanofluids as a cooler for the circular leg structure with 2n-1p segmentation and triangular leg structure with 1n-2p segmentation. The maximum power output of these leg structures with TiO_2 is 0.744 W and 1.064 W, respectively, at a heat flux of 17 kW/m^2.

A change in the sensitivity of the parameters is shown in Figure 14, while the results of Min Li [10] were performed with a $T_c = 20\,^\circ$C, our results are performed with a $T_c = 25\,^\circ$C, the difference of the output power is perceived due to the change in the gradient. The maximum output power of Min Li [10] is 0.326 W, while ours is 0.223 W. In other words, varying the cold side temperature by 5 $^\circ$C can alter the results by up to 32%. Moreover, the difference in efficiency is minimal for this change of gradient, as expected.

Table 7. Output power, efficiency, and exergy for distilled water and TiO_2 used for Min Li's result and for circular and triangular leg structures with different segmentation.

	Output Power (W)	Efficiency	Exergy
Triangular [10]	0.326	0.111	0.338
Triangular 2n-1p	0.907	0.238	0.507
Triangular 1n-1p	0.223	0.107	0.324
Circular 2n-1p	0.634	0.242	0.513
Circular 1n-1p	0.181	0.093	0.322
Triangular [10] TiO_2	0.383	0.130	0.396
Triangular 2n-1p TiO_2	1.064	0.279	0.595
Triangular 1n-1p TiO_2	0.907	0.238	0.507
Circular 2n-1p TiO_2	0.744	0.284	0.598
Circular 1n-1p TiO_2	0.634	0.242	0.513

Finally, it is important to remark that the power output generated by different leg structures can be inverted; for example, Figure 14 shows that the power output of the circular structure and the triangular structure changes for a given value of heat flux. This fact is important for the use of these structures in different operating conditions. If the heat flow is very large, the performance of a structure can improve.

The 12 kW/m² is the critical point of heat flow, it is where the parameters begin to decrease and is due to the properties of the temperature.

For heat flux below 12 kW/m², a circular structure is better than triangular, but if the heat flux is higher than 12 kW/m², the triangular structure is better. The performance between both structures is reversed.

Figure 15 shows how segmenting leg structures can improve thermal efficiency compared to the efficiency obtained by Min Li [10]. For example, at 5 kW/m², the efficiency of Min Li is 4.6%, that of the triangular leg structure with 2n-1p segmentation is 9.111%, and that of the circular model with 2n-1p segmentation is 9.208, improving by up to 200%. For a heat flux of 12 kW/m², the efficiency of Min Li is 9.1%, that of the triangular leg structure with 2n-1p segmentation is 19.57%, and that of the circular leg structure with 2n-1p segmentation is 19.786%. The maximum efficiency is 11.1%, 23.864%, and 24.213%, respectively.
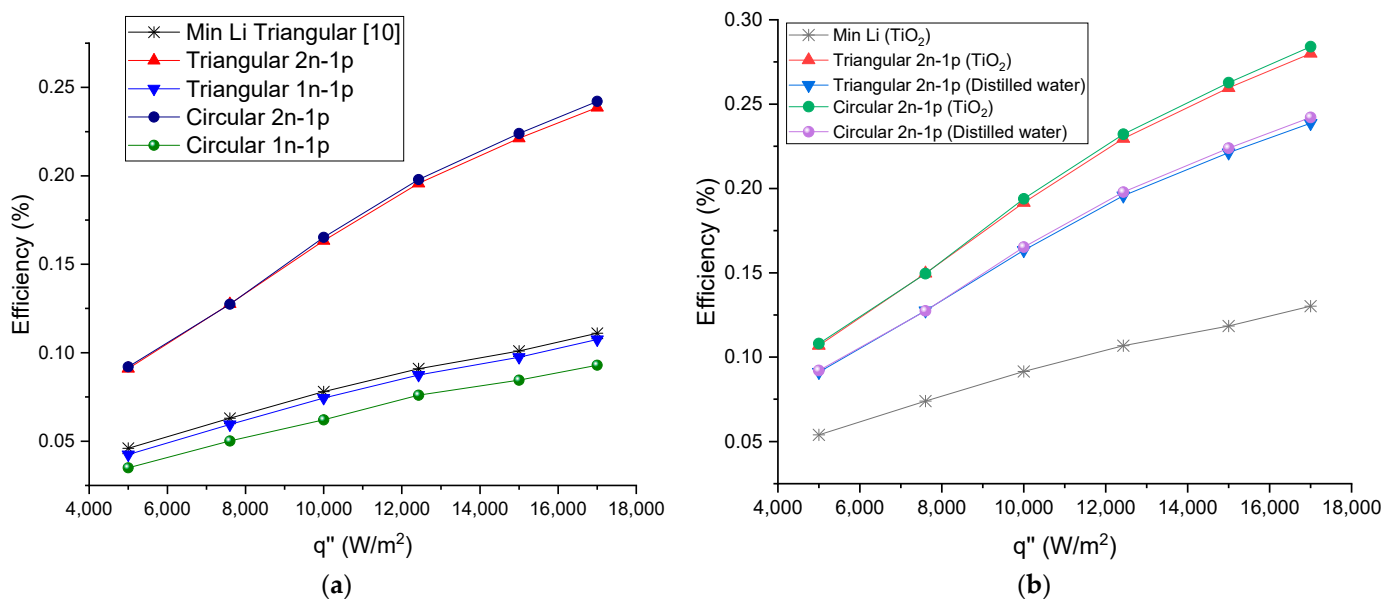
Figure 15. Energy efficiency for circular and triangular leg structures with two different segmentations compared with Min Li results; (**a**) distilled water as coolant and (**b**) TiO_2 as coolant.

The maximum exergy efficiency of Min Li is 0.338, while that of the circular and triangular leg structures with 2n-1p segmentation is 0.513 and 0.507, respectively, improving up to 150%, as shown in Figure 16a. In Figure 16b, before 10 kW/m^2 the exergy efficiency of the segmented models is lower than that of Min Li due to the materials used in the segmentation, but the exergy efficiency improved after 12 kW/m^2. All the results are shown in Table 7.
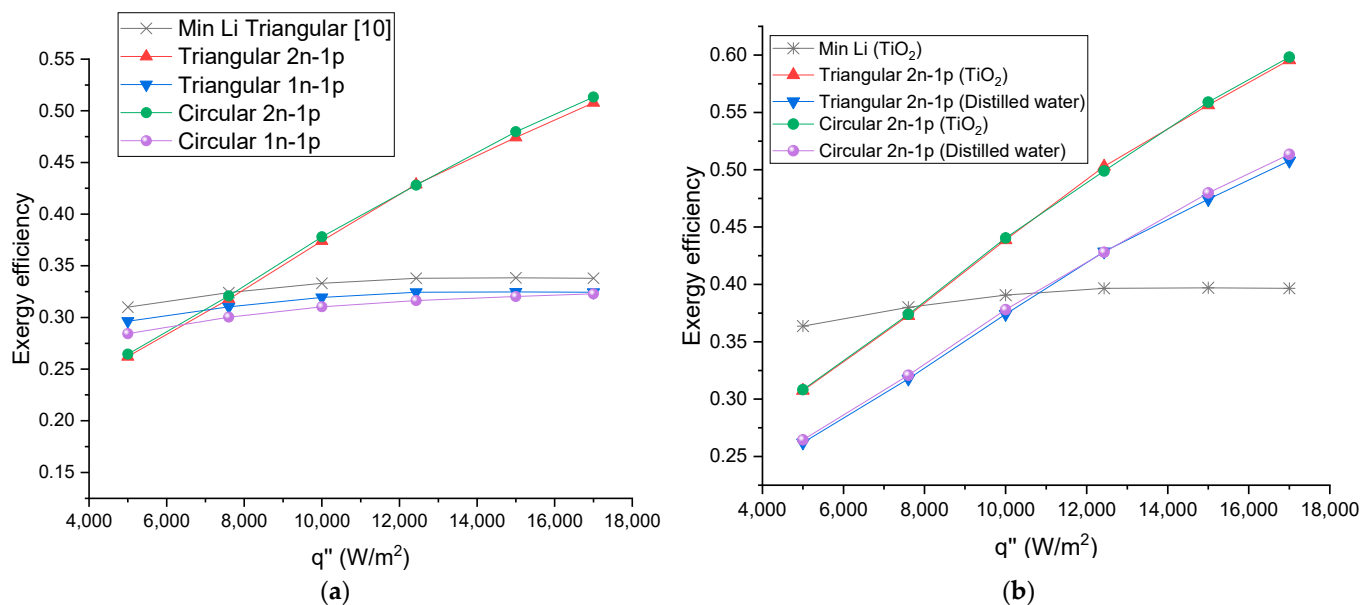

Figure 16. Exergy efficiency for circular and triangular leg structures with two different segmentations compared with Min Li result; (**a**) distilled water as coolant and (**b**) *TiO$_2$* as coolant.

The improvement over the performance of the TEG is small compared with different nanofluids, nevertheless the improvement with nanofluids is bigger compared with distilled water.

The properties of the n-type material contribute to a better performance when material segmentation is considered. Figure A1 of Appendix A shows that the system with segmentation 2n-1p has a better performance than segmentation 1n-2p.

4. Conclusions

The performance of a TEG was studied, performing simulations on an ANSYS Workbench with the thermal-electric module. Temperature-dependent Bi_2Te_3 is used as the semiconductor material of the TEG.

This study focuses on the impact of different cooling nanofluids for optimizing a thermoelectric generator, evaluating its output power, efficiency, and exergy efficiency.

The energy and exergy performance of five different leg structures (square, triangular, circular, octagonal, and rectangular) were analyzed in a stationary state condition.

This study compares the performance of hollow and filled leg structures in a thermoelectric generator using distilled water and various nanofluids as coolants. The results show that the triangular leg structure performs the best in terms of power output, energy conversion, and exergy efficiency, with a maximum efficiency of 0.111 and 0.106 for the hollow and filled leg structures, respectively.

This work demonstrates the improvement in the performance of thermoelectric generators via cooling nanofluids over traditional cooling fluids.

Using nanofluids, the power output, energy conversion, and exergy efficiency improve by 12.57%, 15%, 16.53%, and 17% using Fe_3O_4, graphene, TiO_2, and Al_2O_3 respectively, compared to distilled water.

It is better to use a 2n-1p segmentation to achieve a better output power because the electron charge has a greater capacity to transit around the p-type thermocouples, reaching a maximum P_{out} of 1.064 W. A maximum efficiency of 24.21% was achieved using a 2n-1p segmentation.

Using nanofluids in TEG systems could be a promising way to improve their efficiency and output power. However, more research is needed to investigate the impact of different nanofluids on the performance of TEGs under other operating conditions.

For future research, we strongly suggest the following:

- New materials: researchers can explore and discover new materials with higher thermoelectric performance and lower cost.
- Nanostructuring: research can focus on developing new manufacturing techniques that enable the fabrication of nanostructured materials for thermoelectric generators.
- System-level optimization: Research can be conducted on the system-level optimization of thermoelectric generators. The research can include developing new architectures, optimizing heat transfer and thermal management, and advanced control techniques.

Author Contributions: Conceptualization, M.A.O.-R.; formal analysis, M.A.O.-R.; investigation, M.A.O.-R.; methodology, M.A.O.-R. and C.F.R.-C.; project administration, M.A.O.-R.; resources, L.H.-G.; validation, C.F.R.-C. and L.H.-G.; visualization, C.F.R.-C. and A.E.O.-H.; writing—original draft, C.F.R.-C. and L.H.-G.; writing—review and editing, M.A.O.-R. and A.E.O.-H. All authors have read and agreed to the published version of the manuscript.

Institutional Review Board Statement: Not applicable.

Informed Consent Statement: Informed consent was obtained from all subjects involved in this study.

Data Availability Statement: Data are available upon request due to restrictions, e.g., privacy or ethics. The data presented in this study are available upon request from the corresponding author. However, the data are not publicly available because our research group is still in further research in this area.

Conflicts of Interest: The authors declare no conflict of interest.

Appendix A

For triangular leg structures, the power output and efficiency are analyzed with distilled water and TiO_2. For output power in both cases, it is better when the p-type semiconductor is segmented and the n-type remains of one material. The maximum output power for distilled water and TiO_2 are 0.907 W and 1.064 W, respectively, as shown in Figure A1. The best power output occurs with the 1n-2p segmentation because of the negative charges in the thermocouples.

The maximum efficiencies for distilled water and TiO_2 are 23.86% and 27.99%, respectively (Figure A2). The best efficiency is with the 2n-1p segmentation. The 2n-2p and 1n-2p segmentation start with the same efficiency values, but they separate when they reach a heat flow of 12 Kw/m^2.
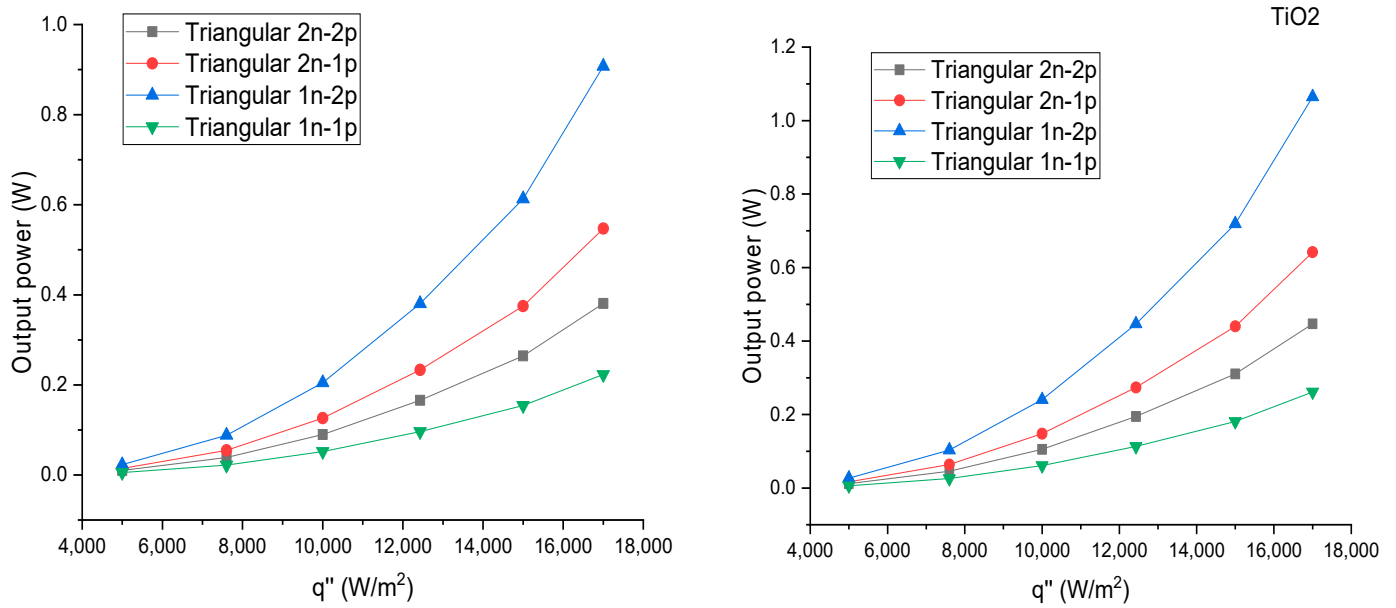
Figure A1. Output power for different cases of segmentation for distilled water and *TiO*$_2$.
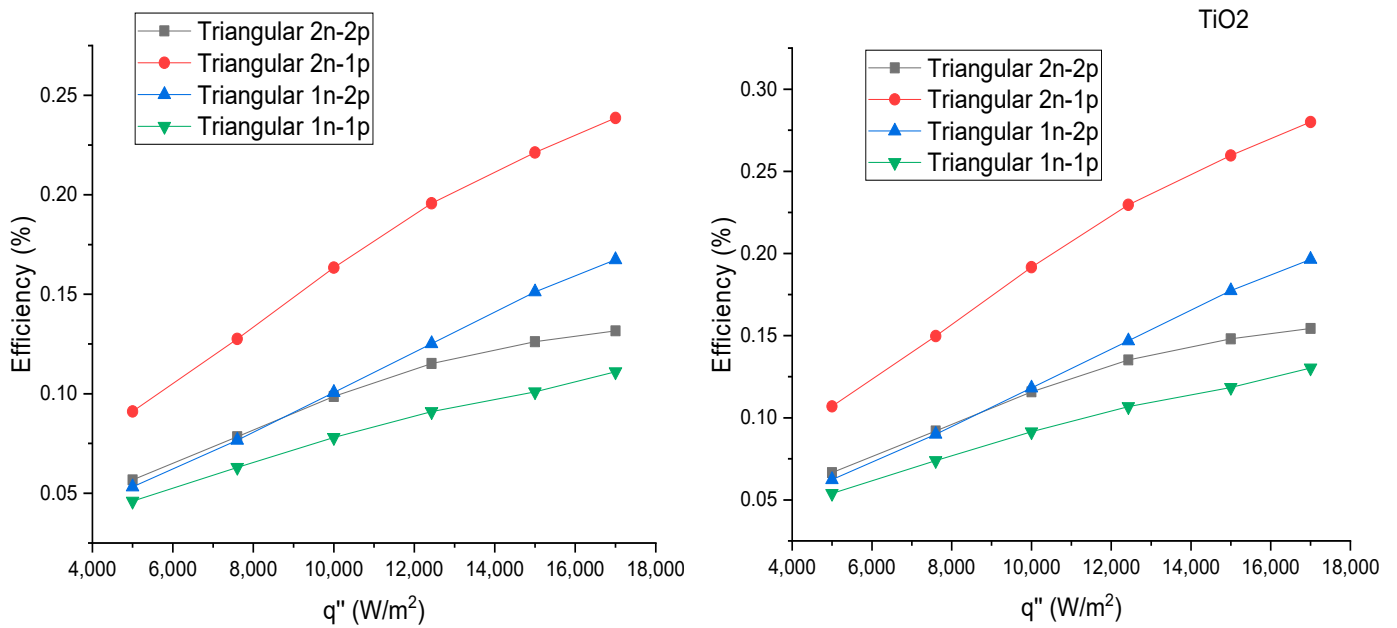

Figure A2. Energy efficiency for different cases of segmentation for distilled water and *TiO*$_2$.

Optimum exergy efficiency is achieved with the 2n-1p segmentation, as shown in Figure A3, with both distilled water quenching and *TiO*$_2$ reaching a maximum exergy efficiency of 0.5759. For the other cases, the exergy decreases. In the case of the segmentation 2n-2p the decrease of exergy efficiency is more noticeable, with the maximum exergy being 0.3402. For the segmented 2n-2p, the behavior is upward, but the maximum exergy is 0.3809.
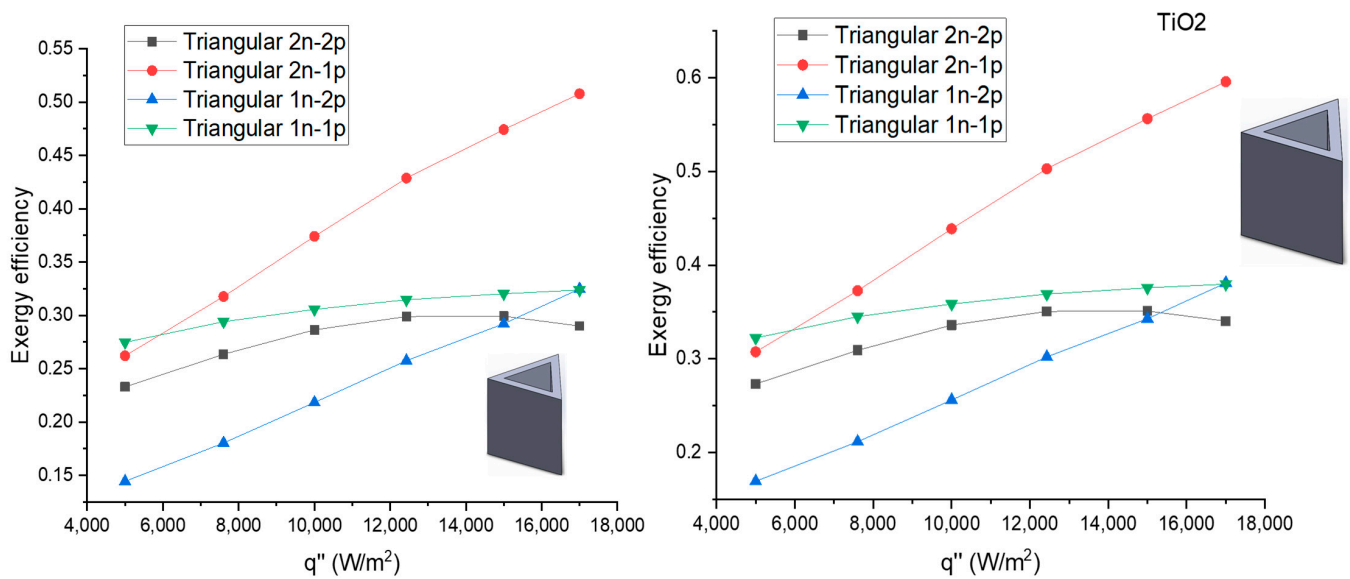
Figure A3. Exergy efficiency for different cases of segmentation for distilled water and *TiO₂*.

References

1. Astrain, D.; Vián, J.G.; Albizua, J. Computational model for refrigerators based on Peltier effect application. *Appl. Therm. Eng.* **2005**, *25*, 3149–3162. [CrossRef]
2. Liao, M.; He, Z.; Jiang, C.; Fan, X.; Li, Y.; Qi, F. A three-dimensional model for thermoelectric generator and the influence of Peltier effect on the performance and heat transfer. *Appl. Therm. Eng.* **2018**, *133*, 493–500. [CrossRef]
3. Deng, W.; Wang, X.; Pan, X.; Zhang, S.; Ding, J.; Li, G. Geometry design and performance optimization of a terrestrial radioisotope thermoelectric generator based on finite element analysis. *Ann. Nucl. Energy* **2021**, *151*, 107883. [CrossRef]
4. Charilaou, K.; Kyratsi, T.; Louca, L.S. Design of an air-cooled thermoelectric generator system through modelling and simulations, for use in cement industries. *Mater. Today Proc.* **2021**, *44*, 3516–3524. [CrossRef]
5. Pourkiaei, S.M.; Ahmadi, M.H.; Sadeghzadeh, M.; Moosavi, S.; Pourfayaz, F.; Chen, L.; Yazdi, M.A.P.; Kumar, R. Thermoelectric cooler and thermoelectric generator devices: A review of present and potential applications, modeling and materials. *Energy* **2019**, *186*, 115849. [CrossRef]
6. Zheng, X.F.; Liu, C.X.; Yan, Y.Y.; Wang, Q. A review of thermoelectrics research—recent developments and potentials for sustainable and renewable energy applications. *Renew. Sustain. Energy Rev.* **2014**, *32*, 486–503. [CrossRef]
7. Shittu, S.; Li, G.; Zhao, X.; Ma, X. Review of thermoelectric geometry and structure optimization for performance enhancement. *Appl. Energy* **2020**, *268*, 115075. [CrossRef]
8. Dongxu, J.; Zhongbao, W.; Pou, J.; Mazzoni, S.; Rajoo, S.; Romagnoli, A. Geometry optimization of thermoelectric modules: Simulation and experimental study. *Energy Convers. Manag.* **2019**, *195*, 236–243. [CrossRef]
9. Chen, W.H.; Wang, C.C.; Hung, C.I.; Yang, C.C.; Juang, R.C. Modeling and simulation for the design of thermal-concentrated solar thermoelectric generator. *Energy* **2014**, *64*, 287–297. [CrossRef]
10. Li, M.; Dizaji, H.S.; Asaadi, S.; Jarad, F.; Anqi, A.E.; Wae-hayee, M. Thermo-economic, exergetic and mechanical analysis of thermoelectric generator with hollow leg structure; impact of leg cross-section shape and hollow-to-filled area ratio. *Case Stud. in Therm. Eng.* **2021**, *27*, 101314. [CrossRef]
11. Lamba, R.; Kaushik, S.C. Thermodynamic analysis of thermoelectric generator including influence of Thomson effect and leg geometry configuration. *Energy Convers. Manag.* **2017**, *144*, 388–398. [CrossRef]
12. Olivares-Robles, M.A.; Badillo-Ruiz, C.A.; Ruiz-Ortega, P.E. A comprehensive analysis on nanostructures materials in a thermoelectric micro-system based on geometric shape, segmentation structure and loas resistance. *Sci. Rep.* **2020**, *10*, 21659. [CrossRef] [PubMed]
13. Thimont, Y.; LeBlanc, S. The impact of thermoelectric leg geometries on thermal resistance and power output. *J. Appl. Phys.* **2019**, *126*, 095101. [CrossRef]
14. Zhao, Y.; Wang, S.; Ge, M.; Li, Y.; Yang, Y. Energy and exergy analysis of thermoelectric generator system with humidified flue gas. *Energy Convers. Manag.* **2018**, *156*, 140–149. [CrossRef]
15. Wiriyasart, S.; Suksusron, P.; Hommalee, C.; Siricharoenpanich, A.; Naphon, P. Heat transfer enhancement of thermoelectric cooling module with nanofluid and ferrofluid as base fluids. *Case Stud. Therm. Eng.* **2021**, *24*, 100877. [CrossRef]
16. Pfeiffelmann, B.; Benim, A.C.; Joos, F. Water-Cooled Thermoelectric Generators for Improved Net Output Power: A Review. *Energies* **2021**, *14*, 8329. [CrossRef]
17. Yang, W.; Zhu, W.; Yang, Y.; Huang, L.; Shi, Y.; Xie, C. Thermoelectric Performance Evaluation and Optimization in a Concentric Annular Thermoelectric Generator under Different Cooling Methods. *Energies* **2022**, *15*, 2231. [CrossRef]

18. Ramos-Castañeda, C.F.; Olivares-Robles, M.A.; Méndez-Méndez, J.V. Analysis of the Performance of a Solar Thermoelectric Generator for Variable Leg Geometry with Nanofluid Cooling. *Processes* **2021**, *9*, 1352. [CrossRef]

19. Abdelkareem, M.A.; Mahmoud, M.S.; Elsaid, K.; Sayed, E.T.; Wilberforce, T.; Al-Murisi, M.; Maghrabie, H.M.; Olabi, A.G. Prospects of Thermoelectric Generators with Nanofluid. *Therm. Sci. Eng. Prog.* **2022**, *29*, 101207. [CrossRef]

20. Ahammed, N.; Asirvatham, L.G.; Wongwises, S. Thermoelectric cooling of electronic devices with nanofluid in a multiport minichannel heat exchanger. *Exp. Therm. Fluid Sci.* **2016**, *74*, 81–90. [CrossRef]

21. Ruan, H.; Xie, H.; Wang, J.; Liao, J.; Sun, L.; Gao, M.; Li, C. Numerical investigation and comparative analysis of nanofluid cooling enhancement for TEG and TEC systems. *Case Stud. Therm. Eng.* **2021**, *27*, 101331. [CrossRef]

22. Xing, J.J.; Wu, Z.H.; Xie, H.Q.; Wang, Y.Y.; Li, Y.H.; Mao, J.H. Performance of thermoelectric generator with graphene nanofluid cooling. *Chin. Phys. B* **2017**, *26*, 104401. [CrossRef]

23. Chen, L.; Yang, C.; Xiao, Y.; Yan, X.; Hu, L.; Eggersdorfer, M.; Chen, D.; Weitz, D.A.; Ye, F. Millifluidics, microfluidics, and nanofluidics: Manipulating fluids at varying length scales. *Mater. Today Nano* **2021**, *16*, 100136. [CrossRef]

24. Sundar, L.S.; Singh, M.K.; Sousa, A.C.M. Investigation of thermal conductivity and viscosity of Fe_3O_4 nanofluid for heat transfer applications. *Int. Commun. Heat Mass Transf.* **2013**, *44*, 7–14. [CrossRef]

25. Kaushik, S.C.; Manikandan, S. The influence of Thomson effect in the energy and exergy efficiency of an annular thermoelectric generator. *Energy Convers. Manag.* **2015**, *103*, 200–207. [CrossRef]

26. Tian, M.W.; Mihardjo, L.W.; Moria, H.; Asaadi, S.; Dizaji, H.S.; Khalilarya, S.; Nguyen, P.T. A comprehensive energy efficiency study of segmented annular thermoelectric generator; thermal, exergetic and economic analysis. *Appl. Therm. Eng.* **2020**, *181*, 115996. [CrossRef]

27. Khedher, N.B.; Selimefendigil, F.; Kolsi, L.; Aich, W.; Ben Said, L.; Boukholda, I. Performance Optimization of a Thermoelectric Device by Using a Shear Thinning Nanofluid and Rotating Cylinder in a Cavity with Ventilation Ports. *Mathematics* **2022**, *10*, 1075. [CrossRef]

28. Ewert, M.K. *Terrestrial, and Aerospace Solar Heat Pump Development: Past, Present, and Future*; ASME: Albuquerque, NM, USA, 1998.

29. Chen, G.; Mu, Y.; Zhai, P.; Li, G.; Zhang, Q. An Investigation on the Coupled Thermal–Mechanical–Electrical Response of Automobile Thermoelectric Materials and Devices. *J. Electron. Mater.* **2013**, *42*, 1762–1770. [CrossRef]

30. Riffat, S.B.; Ma, X. Thermoelectrics: A review of present and potential applications. *Appl. Therm. Eng.* **2003**, *23*, 913–935. [CrossRef]

31. Zhu, L.; Li, H.; Chen, S.; Tian, X.; Kang, X.; Jiang, X.; Qiu, S. Optimization analysis of a segmented thermoelectric generator based on genetic algorithm. *Renew. Energy* **2020**, *156*, 710–718. [CrossRef]

32. Fan, S.; Gao, Y.; Rezania, A. Thermoelectric performance and stress analysis on wearable thermoelectric generator under bending load. *Renew. Energy* **2021**, *173*, 581–595. [CrossRef]

33. Su, X.; Zhang, L.; Liu, Z.; Luo, Y.; Chen, D.; Li, W. Performance evaluation of a novel building envelope integrated with thermoelectric cooler and radiative sky cooler. *Renew. Energy* **2021**, *171*, 1061–1078. [CrossRef]

34. Luo, D.; Yan, Y.; Wang, R.; Zhou, W. Numerical investigation on the dynamic response characteristics of a thermoelectric generator module under transient temperature excitations. *Renew. Energy* **2021**, *170*, 811–823. [CrossRef]

35. Maduabuchi, C.C.; Ejenakevwe, K.A.; Mgbemene, C.A. Performance optimization and thermodynamic analysis of irreversibility in a contemporary solar thermoelectric generator. *Renew. Energy* **2021**, *168*, 1189–1206. [CrossRef]

36. Borhani, S.M.; Hosseini, M.J.; Pakrouh, R.; Ranjbar, A.A.; Nourian, A. Performance enhancement of a thermoelectric harvester with a PCM/Metal foam composite. *Renew. Energy* **2021**, *168*, 1122–1140. [CrossRef]

37. Moaveni, S. *Finite Element Analysis: Theory and Application whit ANSYS*, 4th ed.; Pearson: Noida, India, 2015.